

# Leaving of primordial $\text{Li}^+$ behind forming structures caused by nanogauss magnetic field through an ambipolar diffusion

Motohiko Kusakabe<sup>1\*</sup> † and Masahiro Kawasaki<sup>1,2</sup>

<sup>1</sup>*Institute for Cosmic Ray Research, University of Tokyo, Kashiwa, Chiba 277-8582, Japan*

<sup>2</sup>*Kavli Institute for the Physics and Mathematics of the Universe,  
University of Tokyo, Kashiwa, Chiba 277-8582, Japan*

(Dated: April 1, 2019)

During the structure formation responsible for the Galaxy, charged and neutral chemical species may have separated at the gravitational contraction in primordial magnetic field (PMF). A gradient in the PMF in a direction perpendicular to the field direction leads to the Lorentz force on the charged species. Resultantly, an ambipolar diffusion occurs, and charged species can move differently from neutral species, which collapses gravitationally during the structure formation. We calculate fluid motions of charged and neutral species assuming a gravitational contraction of neutral matter in a spherically symmetric structure. It is shown that the charged fluid, i.e., proton, electron and  ${}^7\text{Li}^+$ , can significantly decouple from the neutral fluid depending on the field amplitude. The charged species can, therefore, escape from the gravitational collapse with neutral species. A narrow parameter region for an effective chemical separation is identified taking the structure mass, the epoch of the gravitational collapse, and the comoving Lorenz force as parameters. This type of chemical separation can reduce the abundance ratio of  $\text{Li}/\text{H}$  in early structures because of inefficient contraction of  ${}^7\text{Li}^+$  ion. The chemical separation may, therefore, explain  $\text{Li}$  abundances of metal-poor stars which are smaller than the prediction in standard big bang nucleosynthesis model. Amplitudes of the PMFs are controlled by a field weakening via magneto-hydrodynamic turbulence. The upper limit on the field amplitude derived from the turbulence is near to the value required for the chemical separation.

PACS numbers: 98.35.Bd, 98.35.Eg, 52.30.Ex, 95.30.Dr

## I. INTRODUCTION

In the standard cosmology, abundances of light elements, i.e., hydrogen, helium, lithium, and very small amounts of other nuclides, stop evolution in the epoch of nucleosynthesis which corresponds to the redshift of  $z \sim 10^9$  [1]. There is, however, a discrepancy in lithium abundances predicted in standard big bang nucleosynthesis (BBN) model [2, 3] and those determined with spectroscopic observations of metal-poor stars (MPSs) [4, 5]. The observational abundance measured by number relative to hydrogen, i.e.,  ${}^7\text{Li}/\text{H} = (1 - 2) \times 10^{-10}$  [4–15], is a factor of 2–4 lower than the prediction in standard BBN (SBBN) model for the baryon-to-photon ratio inferred from the observation of the cosmic microwave background radiation with Wilkinson Microwave Anisotropy Probe (WMAP) [16–19].

When the temperature of the universe decreases, the formations of atom and molecules proceed in the redshift range of  $z \lesssim 10^4$  [20–25]. Since lithium has a low ionization potential, it remains ionized when the recombination of hydrogen occurs [20]. The relic abundance of  $\text{Li}^+$  is, therefore, high [23]. A recent study [25] shows that abundances of  $\text{Li}$  and  $\text{Li}^+$  are almost equal at  $z = 10$ .

On the other hand, it has been known that magnetic fields exist in many astronomical objects of varying sizes, such as Sun, Galaxy, galactic cluster (see [26] for a review). Such magnetic fields can be generated through electric currents induced by a difference in velocities of electron and ion [27, 28]. The electric current is produced in a rotating gas system because of different viscous resistances of electron and ion [28]. This current then creates poloidal magnetic field. Similarly, the field generation from the drift current produced through gravitations operating to electrons and ions has been suggested [28–30]. It was thereafter noted [31] that the batteries [27, 28] can not generate a large magnetic field since the time scale of field generation is much larger than the age of the universe [31–33].

Many epochs in the early universe have been studied in efforts to find possible causes of the primordial magnetic field (PMF). They include the inflation, electroweak and quark-hadron transitions, and reionization (see Refs. [26, 34, 35] and references therein). Among them, the most probable epoch is shortly before and after the decoupling of matter and cosmic background radiation (CBR), and recombination of proton and electron [36–43]. In the evolution of primordial density perturbation, the magnetic field can be generated at second order through the vorticity [42] and

---

\* Present address: School of Liberal Arts and Science, Korea Aerospace University, Goyang 412-791, Korea, and Department of Physics, Soongsil University, Seoul 156-743, Korea

† motohiko@kau.ac.kr

the anisotropic stress of photon [38, 40]. The effect of these processes can be calculated rather precisely with the cosmological perturbation theory, using model parameter values which are significantly constrained from observations of CBR. Recently, the magnetic field generation has been calculated completely taking account of all important terms [37]. According to their result, the value of generated comoving field measured at redshift  $z = 0$  on cluster scales, i.e., 1 Mpc, is about  $3 \times 10^{-29}$  G.

Effects of PMFs on Galaxy formation have been studied [44–46], and effects on Galactic angular momentum and Galactic magnetic fields have been also investigated utilizing magneto-hydrodynamic (MHD) equations to treat the early universe [45, 46]. It was found that when a structure with a scale  $L_B$  forms, the magnetic field of amplitude in the present intergalactic medium (IGM),  $B_0(L_B) \sim 10^{-9}(L_B/1 \text{ Mpc})$  G, causes an overdensity of  $\delta = 1$  [45, 46]. It has been suggested that an inhomogeneous magnetic field causes a streaming velocity of baryon relative to dark matter, which may result in an inhibition of an infall of baryon in potential wells of dark matter, and affect cosmological structure formation [46].

In this paper, we study a chemical separation of charged and neutral species triggered by a PMF during the structure formation. If there is a gradient in the PMF in a direction perpendicular to the field direction in the early universe, an electric current of charged species also exists in the direction perpendicular to both directions of the field lines and the gradient. The Lorentz force working on the charged species then causes a velocity difference between charged and neutral species in the direction of the field gradient. This velocity difference enables an ambipolar diffusion, and a motion of charged species possibly decouples from that of neutral species which collapses gravitationally during the structure formation. Because of this process,  ${}^7\text{Li}^+$  ions may have gotten left behind structures while neutral  ${}^7\text{Li}$  atoms gravitationally collapsed into structures. We suggest that the ambipolar diffusion provides a possible explanation of the Li abundance in MPSs.

The organization of this paper is as follows. In Sec. II we describe the model of chemical separation during a gravitational collapse of a structure. In Sec. III we introduce physical quantities used in this study, and typical numerical values relevant to the structure formation. In Sec. IV we show results of calculations of the chemical separation caused by the magnetic field. In Sec. V we comment on the magnetic field amplitude. In Sec. VI we identify a parameter region required for a successful chemical separation. In Sec. VII we mention a later epoch of the structure formation and possible reactions which are both not treated in this study. We suggest that the chemical separation of the  ${}^7\text{Li}^+$  ion can reduce the abundance ratio  ${}^7\text{Li}/\text{H}$  in the early structure. Another theoretical constraint on the magnetic field amplitude is also described. In Sec. VIII we summarize this study. In Appendix A we show drift velocities of proton and electron in a structure, equations for ions and electron to be satisfied in equilibrium states, and typical values of variables for an efficient chemical separation. In Appendix B we show supplemental results of the calculations of the chemical separation. In this paper, the Boltzmann’s constant ( $k_B$ ) and the light speed ( $c$ ) are normalized to be unity.

## II. MODEL

We focus on the leaving of ionic species behind forming structures at redshift  $z = \mathcal{O}(10)$ . First, the initial state of model structure has a uniform density and parallel magnetic field whose amplitude has a gradient in a direction perpendicular to the field lines. This simple condition is assumed to just suggest that ionized chemical species can have bulk velocities different from that of neutral hydrogen. The magnetic field of typical volume scale of the structure has been likely generated by motions of charged species which exist outside the structure originally. In order to precisely follow the evolution for the spatial distribution of magnetic field in the structure, the evolution of electric circuit including both inside and outside of the structure should be considered [47]. In this calculation, however, we do not treat the outer region, and use a boundary condition. Second, the structure is modeled as an axisymmetric structure in a cylindrical coordinate system  $(r, \phi, z)$  with an axis of symmetry taken to be  $z$ -axis. Azimuthal components of all physical quantities, therefore, do not depend on the azimuthal angle  $\phi$ . The outer edge of the structure exists at  $r = r_{\text{str}}$ .

Figure 1 is an illustration of the physical concept of chemical separation studied in this paper. In the left panel, the large solid circle is a boundary of a structure collapsing gravitationally, thin arrows are magnetic field lines, and open arrows are gravitational accelerations. Since the axial symmetry has been assumed, this structure itself can be roughly regarded as a large coil as shown with a dashed lines. The right panel shows an enlarged view of the cross section of the structure. The three axis of the cylindrical coordinate are defined in the panel. A magnetic field exits along the  $z$ -axis (the thin arrow), and the magnetic field amplitude has a gradient in the  $-r$  direction (the filled thick arrow). Then, there is a  $\phi$  component of the  $\nabla \times \mathbf{B}$  term or an azimuthal electric current (mark  $\otimes$ ). The combination of this current and the magnetic field generates the Lorentz force ( $\mathbf{F}_L$ ) on the charged fluid in the  $r$  direction. Resultantly, the charged fluid has a radial velocity relative to the neutral fluid. The Lorentz force is then balanced with a friction force by neutral fluid which depends on the radial relative velocity ( $\mathbf{F}_{\text{fric}}$ ).

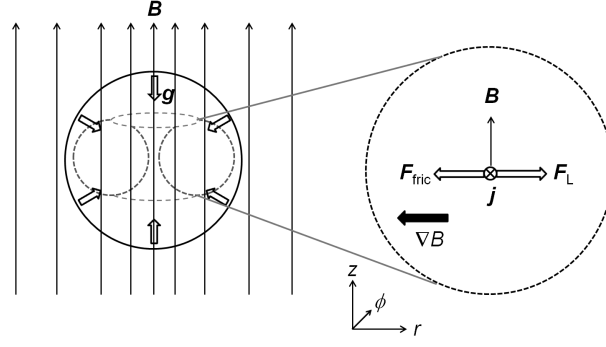


FIG. 1: Illustration of chemical separation in a collapsing structure. In the left panel, the large solid circle delineates a collapsing structure, thin arrows are magnetic field lines, and open arrows are gravitational accelerations. The structure is axisymmetric with respect to the field direction, and can be seen as a large coil shown with a dashed lines. The right panel shows an enlarged view of the cross section of the structure with the three axis of the cylindrical coordinate defined. We assume a magnetic field along the  $z$ -axis (the thin arrow), and a gradient in the field amplitude in the  $-r$  direction (the filled thick arrow). There is a  $\phi$  component of the  $\nabla \times \mathbf{B}$  term or an azimuthal electric current (mark  $\otimes$ ). Charged fluid with this current in the magnetic field receives the Lorentz force ( $\mathbf{F}_L$ ) in the  $r$  direction. Resultantly, the charged fluid has a radial velocity relative to the neutral fluid. The Lorentz force is then balanced with a friction force by neutral fluid ( $\mathbf{F}_{\text{fric}}$ ).

### A. Fluid and electromagnetic equations

The following equations are adopted.

- equation of continuity for neutral matter:

$$\frac{\partial \rho_n}{\partial t} + \nabla \cdot (\rho_n \mathbf{v}_n) = 0, \quad (1)$$

where  $\rho_n$  and  $\mathbf{v}_n$  are the density and fluid velocity of the neutral matter composed mainly of neutral hydrogen, and  $t$  is the cosmic time.

- equation of continuity for ionized species  $i$ :

$$\frac{\partial \rho_i}{\partial t} + \nabla \cdot (\rho_i \mathbf{v}_i) = 0, \quad (2)$$

where  $\rho_i$  and  $\mathbf{v}_i$  are the density and the velocity of species  $i$ . The finite differential expression in the cylindrical coordinate system is

$$\frac{\Delta \rho_i}{\Delta t} = -\frac{1}{r} \frac{\Delta (r \rho_i v_{ir})}{\Delta r} - \frac{\Delta (\rho_i v_{iz})}{\Delta z}. \quad (3)$$

- force equations of proton and electron:

Equations of motion are given by

$$\frac{D\mathbf{v}_p}{Dt} = -\frac{1}{\rho_p} \nabla P_p + \frac{e}{m_p} (\mathbf{E} + \mathbf{v}_p \times \mathbf{B}) + \frac{1}{\tau_{pn}} (\mathbf{v}_n - \mathbf{v}_p) + \frac{1}{\tau_{pe}} (\mathbf{v}_e - \mathbf{v}_p), \quad (4)$$

$$\frac{D\mathbf{v}_e}{Dt} = -\frac{1}{\rho_e} \nabla P_e - \frac{e}{m_e} (\mathbf{E} + \mathbf{v}_e \times \mathbf{B}) + \frac{1}{\tau_{en}} (\mathbf{v}_n - \mathbf{v}_e) - \frac{1}{\tau_{ep}} (\mathbf{v}_e - \mathbf{v}_p), \quad (5)$$

where  $D/(Dt)$  is the material time-derivative,  $\mathbf{v}_i$ ,  $P_i$ , and  $m_i$  are the velocity, pressure, and particle mass, respectively, of species  $i$ ,  $e$  is the electronic charge,  $\mathbf{E}$  is the electric field,  $\mathbf{B} = (B_r, B_\phi, B_z)$  is the magnetic field in a cylindrical coordinate, and  $\tau_{ij}^{-1}$  is the energy loss rate of  $i$  through the scattering with  $j$ , or the slowing-down rate of relative velocity of  $i$  and  $j$  [cf. Eq. (53)]. In the balance equations of charged species, a

term of cosmological redshift is neglected since the time scale relevant to the redshift is much larger than those for others. We neglect terms of pressure gradient in this paper. The force equations then reduce to the form of

$$\mathbf{E} = -\mathbf{v}_p \times \mathbf{B} - \frac{\rho_p}{\tau_{pn}} \frac{(\mathbf{v}_n - \mathbf{v}_p)}{en_p} - \frac{\rho_p}{\tau_{pe}} \frac{(\mathbf{v}_e - \mathbf{v}_p)}{en_p}, \quad (6)$$

$$\mathbf{E} = -\mathbf{v}_e \times \mathbf{B} + \frac{\rho_e}{\tau_{en}} \frac{(\mathbf{v}_n - \mathbf{v}_e)}{en_e} - \frac{\rho_e}{\tau_{ep}} \frac{(\mathbf{v}_e - \mathbf{v}_p)}{en_e}. \quad (7)$$

We note that we neglected an effect of  $\nabla B$  drift since it would be small. The force of  $\nabla B$  is given by

$$\begin{aligned} F_{\nabla B} &= \left| -\frac{m_i v_{i\perp}^2 \nabla B}{2B} \right| \\ &= 1.55 \times 10^{-47} \text{ GeV}^2 \left( \frac{m_i}{\text{GeV}} \right) \left( \frac{v_{i\perp}}{2.20 \times 10^{-6}} \right)^2 \left( \frac{\nabla B/B}{\text{kpc}^{-1}} \right), \end{aligned} \quad (8)$$

where  $v_{i\perp}$  is the velocity of  $i$  perpendicular to the  $\mathbf{B}$  direction. On the other hand, the friction force from neutral species on charged species is given by

$$\begin{aligned} F_{\text{fric}} &= \left| \frac{m_i (\mathbf{v}_n - \mathbf{v}_i)}{\tau_{in}} \right| \\ &= 2.01 \times 10^{-41} \text{ GeV}^2 \left( \frac{m_i}{\text{GeV}} \right) \left( \frac{v_{nr} - v_{ir}}{1.61 \text{ km s}^{-1}} \right) \left( \frac{n_H}{5.69 \times 10^{-3} \text{ cm}^{-3}} \right) \left[ \frac{(\sigma v)_{in}}{10^{-9} \text{ cm}^3 \text{ s}^{-1}} \right], \end{aligned} \quad (9)$$

where  $(\sigma v)_{ij}$  is the momentum transfer cross section  $\sigma$  times velocity  $v$  in the reaction of  $i+j$  [cf. Eq. (51)]. Since the equation  $F_{\text{fric}} \gg F_{\nabla B}$  holds, the effect of the gradient in magnetic field is much smaller than that of the friction.

- Faraday's law of induction:

$$\frac{\partial \mathbf{B}}{\partial t} = -\nabla \times \mathbf{E}. \quad (10)$$

The following equation is derived with Eqs. (6) and (10)

$$\frac{\partial \mathbf{B}}{\partial t} = \nabla \times (\mathbf{v}_p \times \mathbf{B}) - \frac{m_p}{e} \nabla \times \left[ \frac{(\mathbf{v}_p - \mathbf{v}_n)}{\tau_{pn}} + \frac{(\mathbf{v}_p - \mathbf{v}_e)}{\tau_{pe}} \right]. \quad (11)$$

Note that the azimuthal component of magnetic field is always much smaller than  $B_z$  in the setup of this study.

- electric current density:

$$\mathbf{j} = en_p \mathbf{v}_p - en_e \mathbf{v}_e. \quad (12)$$

The Lorentz force term in Eq. (19) is balanced with the friction term from neutral matter [cf. Eqs. (6), (7) and (12)]:

$$\mathbf{j} \times \mathbf{B} = \frac{\rho_p}{\tau_{pn}} (\mathbf{v}_p - \mathbf{v}_n) + \frac{\rho_e}{\tau_{en}} (\mathbf{v}_e - \mathbf{v}_n), \quad (13)$$

In the steady state, the balance of force in the radial direction leads to

$$j_\phi B_z = en_p (\alpha_{pn} + \alpha_{en}) (v_{pr} - v_{nr}), \quad (14)$$

where the conditions  $n_p = n_e$  and  $j_r = j_z = 0$  were assumed, and  $\alpha_{ij} = m_i / (e\tau_{ij})$  was defined.

- Ampere's law

$$\nabla \times \mathbf{B} = 4\pi \mathbf{j} \quad (15)$$

- Gauss's law for magnetism:

$$\nabla \cdot \mathbf{B} = 0. \quad (16)$$

The divergence of the Maxwell-Faraday equation [Eq. (10)] is given by

$$\frac{\partial(\nabla \cdot \mathbf{B})}{\partial t} = -\nabla \cdot (\nabla \times \mathbf{E}) = 0. \quad (17)$$

When the Gauss's law is satisfied in the initial condition, it remains satisfied because of this equation.

- force equation of neutral matter:

When the pressure gradient term is neglected, the force equation for neutral particles is given [48] by

$$\frac{\partial(\rho_n \mathbf{v}_n)}{\partial t} + \nabla \cdot (\rho_n \mathbf{v}_n \mathbf{v}_n) = \rho_n \mathbf{g} + \frac{\rho_n}{\tau_{np}} (\mathbf{v}_p - \mathbf{v}_n) + \frac{\rho_n}{\tau_{ne}} (\mathbf{v}_e - \mathbf{v}_n), \quad (18)$$

where  $\mathbf{g}$  is the gravitational acceleration. The second and third terms in the right-hand side (RHS) are for frictions from proton and electron, respectively, working on the neutral particles. Using the balance of the Lorentz force and friction force [Eq. (13)], the Ampere's equation [Eq. (15)], and the Newton's law of action and reaction [Eq. (58)], we can transform the friction terms to the Lorentz-force term [48]:

$$\frac{\partial(\rho_n \mathbf{v}_n)}{\partial t} + \nabla \cdot (\rho_n \mathbf{v}_n \mathbf{v}_n) = \rho_n \mathbf{g} + \frac{(\nabla \times \mathbf{B}) \times \mathbf{B}}{4\pi}. \quad (19)$$

When the azimuthal component of magnetic field is negligibly small, i.e.,  $B_\phi = 0$ , the second term in RHS is described as

$$(\nabla \times \mathbf{B}) \times \mathbf{B} = \left( \frac{\partial B_r}{\partial z} - \frac{\partial B_z}{\partial r} \right) \begin{pmatrix} B_z \\ 0 \\ -B_r \end{pmatrix}. \quad (20)$$

Under the spherical symmetry, the gravitational acceleration is given by

$$\begin{aligned} |\mathbf{g}(\mathbf{r}_p)| = g(r_{\text{str}}) &= G \frac{M(r_{\text{str}})}{r_{\text{str}}^2} = G \left( \frac{4\pi}{3} \right)^{2/3} \rho_m^{2/3} M_{\text{str}}^{1/3} \\ &= 3.93 \times 10^{-11} \text{ cm s}^{-2} \left( \frac{\rho_m}{7.64 \times 10^{-26} \text{ g cm}^{-3}} \right)^{2/3} \left( \frac{M_{\text{str}}}{10^6 M_\odot} \right)^{1/3}, \end{aligned} \quad (21)$$

where  $\mathbf{r}_p$  is the position vector from the center of sphere in a spherical coordinate,  $r_{\text{str}}$  is the radius at the edge of the structure,  $G$  is the gravitational constant,  $M(r_p)$  is the mass contained inside the radius  $r_p$ ,  $\rho_m$  is the matter density, and  $M_{\text{str}}$  is the mass of the structure. In the equation the energy density is normalized to the value at the turnround ( $z_{\text{tur}} = 16.5$ ; see Sec. III).

The amplitude of the first term in RHS of Eq. (19) for gravitation is estimated to be

$$\begin{aligned} \rho_n g &\simeq \rho_b g \\ &= 1.90 \times 10^{-88} \text{ GeV}^5 \left( \frac{\rho_b}{1.27 \times 10^{-26} \text{ g cm}^{-3}} \right) \left( \frac{\rho_m}{7.64 \times 10^{-26} \text{ g cm}^{-3}} \right)^{2/3} \left( \frac{M_{\text{str}}}{10^6 M_\odot} \right)^{1/3}, \end{aligned} \quad (22)$$

where  $\rho_b$  is the baryon density.

The amplitude of the second term in RHS of Eq. (19) for the Lorentz force is estimated to be

$$\begin{aligned} \left| \frac{(\nabla \times \mathbf{B}) \times \mathbf{B}}{4\pi} \right| &\sim \frac{1}{4\pi} \frac{B^2}{L_B} \\ &= 4.09 \times 10^{-89} \text{ GeV}^5 \left( \frac{B}{10^{-7} \text{ G}} \right)^2 \left( \frac{L_B}{597 \text{ pc}} \right)^{-1}, \end{aligned} \quad (23)$$

where  $L_B$  is the length scale of coherent magnetic field.

## B. Galactic infall model

We assume that the second term in RHS of Eq. (19) is negligible, and that the initial density is exactly uniform inside a sphere as a toy model of collapsing structure. In this setup, Eqs. (1) and (19) have spherical symmetry, and Eq. (19) reduces to a free fall of spherical material. A gas heating associated with virialization is neglected, and the gas temperature is assumed to evolve adiabatically after it decoupled from the CBR temperature at  $z \sim 200$  [52]. It is then given by  $T = 2.3 \text{ K}[(1+z)(1+\delta)^{1/3}/10]^2$ , where

$$\delta \equiv (\rho_m - \bar{\rho}_m)/\bar{\rho}_m \quad (24)$$

is the ratio of overdensity of matter relative to the cosmological average density  $\bar{\rho}_m$  [53]. We assume that the baryon density is proportional to the matter density. This approximation is good as long as any radiative astrophysical object such as first stars does not form yet.

The free fall of the sphere under an environment affected by a self gravity is described by the Lagrangian equation of motion, i.e.,  $\partial^2 r_p / \partial t^2 = -GM(r_p)/r_p^2$  [54]. The radius and velocity are then related to the time  $t$  as described [54] by

$$r_p = A_G(1 - \cos \theta), \quad (25)$$

$$t = B_G(\theta - \sin \theta), \quad (26)$$

$$v_n = \frac{\partial r_p}{\partial t} = \frac{A_G}{B_G} \frac{\sin \theta}{1 - \cos \theta}, \quad (27)$$

where the condition  $A_G^3 = GMB_G^2$  is satisfied. The velocity evolution,  $v_n(t) = |\mathbf{v}_n(t)|$ , is given by this equation set. The assumption of the initial uniform density corresponds to  $B_G = \text{constant}$  for any  $A_G$ . The velocity then depends only on the radius parameter  $A_G$ . In this case, the density is always independent of the spatial coordinate, and each mass shell satisfies

$$\rho_n(t) = \rho_{n,i} [r_{pi}/r_p(t)]^3, \quad (28)$$

where  $\rho_n(t)$  and  $\rho_{n,i}$  are the densities at time  $t$  and initial time  $t_i$ , respectively, and  $r_{pi}$  is the radius at initial time.

For a given value of time  $t$ , a value of  $\theta$  and corresponding values of  $r_p$  and  $v_n$  are derived.

## C. Velocities of charged species

For the system composed mainly of proton, electron, and neutral matter, the total plasma force equation holds [48]:

$$\frac{\rho_n}{\tau_{np}} (\mathbf{v}_p - \mathbf{v}_n) + \frac{\rho_n}{\tau_{ne}} (\mathbf{v}_e - \mathbf{v}_n) = \frac{(\nabla \times \mathbf{B}) \times \mathbf{B}}{4\pi}. \quad (29)$$

Thus, a velocity difference of charged and neutral species is related to the Lorentz force operating on whole charged species composed mostly of proton and electron. Matters in astrophysical objects are nearly complete charge-neutral. We, therefore, assume that fluid velocities of proton and electron are equal as for  $r$ - and  $z$ -components. Charged species are then considered as one component as long as motions in  $r$ - and  $z$ -directions are concerned. Since the proton density is larger than the electron density by a factor of  $m_p/m_e = 1836$ , the friction on proton is the predominant friction working on total charged fluid. A balance of the friction and the Lorentz force gives a relation:

$$\mathbf{v}_{p,(rz)} = \mathbf{v}_{n,(rz)} + \frac{\tau_{np}}{(1 + \tau_{np}/\tau_{ne}) \rho_n} \frac{[(\nabla \times \mathbf{B}) \times \mathbf{B}]_{,(rz)}}{4\pi}, \quad (30)$$

where vector components in the  $r$ - $z$  plane are represented by subscript  $(rz)$ . The factor  $(1 + \tau_{np}/\tau_{ne})$  in denominator is neglected because of  $\tau_{np}/\tau_{ne} \ll 1$ .

The  $\phi$ -component of Eq. (29), on the other hand, does not give an equation with  $v_{p\phi}$  when the relation between  $v_{p\phi}$  and  $v_{e\phi}$  [Eq. (A7)] is satisfied. In this case, terms of  $v_{p\phi}$  and  $v_{e\phi}$  cancel with each others [cf. Eqs. (53) and (58)]. The equation then reduces to

$$\rho_n \left( \frac{1}{\tau_{np}} + \frac{1}{\tau_{ne}} \right) v_{n\phi} + \frac{[(\nabla \times \mathbf{B}) \times \mathbf{B}]_{\phi}}{4\pi} = 0. \quad (31)$$

TABLE I: Mass of chemical species

species	mass (GeV)
H	0.9387829835247
H <sup>+</sup>	0.9382719982211
Li	6.5353662335057
Li <sup>+</sup>	6.5348552399954

The proton velocity  $\mathbf{v}_p$  is derived from the rotation of magnetic field  $\nabla \times \mathbf{B}$  using the Ampere's equation [Eq. (15)], as in studies of molecular clouds (MCs) [48–51]. The rotation of the magnetic field is related to the electric current density, which both have existed from the start time of calculation (see Sec. V). Using Eqs. (12) for the current density and (A7) for the relation between velocities of proton and electron, the  $\phi$ -component of the Ampere's equation gives the azimuthal proton velocity as

$$v_{p\phi} = \frac{\partial_z B_r - \partial_r B_z}{4\pi en_p(1 + \alpha_{pn}/\alpha_{en})}. \quad (32)$$

The assumption of  $v_{pr} = v_{er}$  and  $v_{pz} = v_{ez}$  correspond to no current densities in the  $r$ - and  $z$ -directions. Constraints on velocities of charged species in the  $r$ - $z$  plane are, therefore, not given through the Ampere's equation.

#### D. Atomic mass and cross section data

Table I shows adopted masses of atoms and ions, i.e.,  $i$ , which are derived with atomic and electronic mass data [55, 56], and ionization energies of  $i$  or binding energies of  $i^+$  and  $e^-$ ,  $\text{BE}(i^+, e)$  [57]:  $\text{BE}(\text{H}^+, e) = 13.5984$  eV [58] and  $\text{BE}(\text{Li}^+, e) = 5.3917$  eV [59].

Reaction cross sections  $\sigma_{in}$  are taken from Refs. [60, 61] for  $i = \text{H}^+$  and Ref. [62] for  ${}^7\text{Li}^+$ . Linear interpolations are utilized taking velocities as parameters. Cross sections for energies lower than the minimum energy of data ( $E_{\min}$ ) are given by the value at the energy  $E = E_{\min}$ , while those for energies larger than the maximum energy ( $E_{\max}$ ) are given by the value at  $E = E_{\max}$ .

#### E. Initial conditions

We take a typical comoving magnetic field value  $B_{z0}$  as an input parameter. The initial magnetic field is then assumed to be  $B_{zz_i}(r) = B_{z0}(1 + z_i)^2(1.5 - r/r_{\text{str}})$  for  $0 \leq r \leq 1.4r_{\text{str}}$  and  $B_{zz_i}(r) = 0.1B_{z0}(1 + z_i)^2$  for  $1.4r_{\text{str}} \leq r$ , where  $B_{zz_i}(r)$  is the  $z$ -component of magnetic field in IGM at the initial redshift  $z_i$  at radius  $r$ .

As for initial velocities of proton and  $\text{Li}^+$ , radial and  $z$ -components are assumed to be the same as those of hydrogen. The  $\phi$ -component of proton velocity is given by Eq. (32) with the initial  $\mathbf{B}(r)$  distribution.

Initial chemical abundances are taken from values at  $z = 10$  calculated in the model of homogeneous universe [25]:  $\text{H}^+/\text{H} = 6.52 \times 10^{-5}$ , and  $\text{Li}^+/\text{Li} = 1.0$ . We assume the Li nuclear abundance in SBBN model,  $\text{Li}/\text{H} = 5.2 \times 10^{-10}$  [64]. The chemical number fractions relative to hydrogen are then given by  $\text{H}^+/\text{H} = 6.52 \times 10^{-5}$ ,  $\text{Li}/\text{H} = 2.6 \times 10^{-10}$ , and  $\text{Li}^+/\text{H} = 2.6 \times 10^{-10}$ . A precise calculation of ionic motions should include chemical reactions coupled to the hydrodynamical calculation of the structure formation. This is, however, beyond the scope of this paper.

#### F. Boundary conditions

Boundary conditions are important to describe plasma motions since a plasma inside a region is affected by not only physical parameters inside the region but also those outside the region [47]. We adopt the following conditions. Radial components of velocities of any species  $j$  are zero on the axis of symmetry:

$$v_{jr}(r = 0) = 0. \quad (33)$$

The density, recession velocity of neutral hydrogen, and number fractions of chemical species are initially given by the cosmic average values. Outside the structure, the magnetic field is supposed to be homogeneous in the  $z$ -direction with its value evolving by redshift in the homogeneous universe. We, however, just assume that physical variables



such as ion velocities connect smoothly at the Galactic boundary, and do not treat the conjunction. Calculations are performed under the assumption of a contraction of material with a homogeneous overdensity of infinite size.

As for a treatment for edges of computation domain, an origin and outer edges are defined. Because of the symmetry, constraints on velocities  $v_j = 0$  (for any  $j$ ) always holds at the origin. In every time step we reset values of  $\rho_i$  and  $\mathbf{B}$  at  $r = 0$  ( $z$ -axis) and on the plane of  $z = 0$  to be values calculated for the next innermost grid points, i.e.,  $r = \Delta r$  and  $z = \Delta z$ , respectively. Values of  $\rho_i$  and  $\mathbf{B}$  on an outer edge plane are always given by the average value of collapsing matter. Because of the axial symmetry, the radial and azimuthal components of magnetic field are zero on  $z$  axis. At outer edge points of maximum  $r$  and  $z$  values, the densities of proton, electron, and  ${}^7\text{Li}^+$  are fixed with values derived in the assumption of homogeneous contraction. In addition, at the edge points of  $r = r_{\text{str}}$  the magnetic field components are fixed as  $B_r = 0$ ,  $B_\phi = 0$ , and  $B_{zz}(r_{\text{str}}) = 0.1B_{z0}(1+z)^2(1+\delta)^{2/3}$ .

### G. Calculation

The time step is determined so that changes in magnetic field and densities of ionized species in each step are much smaller than their amplitudes. In performing the time integration of variables  $A(a)$ , spatial differentiation is estimated with a finite difference method using the central difference. The difference is derived from quantities evaluated at intermediate positions between grid points with intervals of  $\Delta a$ , i.e.,  $\partial A(a)/\partial a = [A(a + \Delta a/2) - A(a - \Delta a/2)]/\Delta a$ . The number of grid point is 260 ( $r$  direction)  $\times$  102 ( $z$  direction) and the spacing is  $\Delta r = \Delta z = 5.97$  pc. The computational region is, therefore,  $0 \leq r \leq 1.55$  kpc and  $0 \leq z \leq 0.603$  kpc. The initial time is 9.29Myr, and the ending time is 474Myr, respectively after big bang.

In our calculation code, time evolutions of physical variables are calculated as follows. For a time  $t$ , the velocity [Eq. (27)] and the density [Eq. (28)] of neutral matter, the overdensity of matter [Eq. (24)] and the temperature [Eq. (45)] are derived. For respective reactions, the code evaluate relative velocities determined from thermal mean velocities [Eq. (52)] and relative fluid velocities. Then, the friction time scales [Eqs. (51) and (54)] and the friction parameters [Eq. (53)] are derived with the law of action and reaction [Eq. (58)]. Besides, the electric field [Eqs. (A4–A6)], the velocities of proton [Eqs. (30) and (32)], electron [Eq. (A7)], and  $\text{Li}^+$  [Eq. (A15)] are calculated. Finally, the magnetic field [Eq. (11)] and the densities of charged species [Eq. (3)] are obtained by time integrations of their change rates.

## III. PHYSICAL QUANTITIES

- cosmological parameters

The  $\Lambda$ CDM (dark energy  $\Lambda$  and cold dark matter) model is adopted for the cosmic expansion history. Parameter values are taken from analysis of WMAP9 CBR data ( $\Lambda$ CDM model [19]) [83]: The Hubble parameter is  $H_0 = 70.0 \pm 2.2$  km s $^{-1}$ Mpc $^{-1}$ , and energy density parameters of matter and baryon are  $\Omega_m = 0.279 \pm 0.025$  and  $\Omega_b = 0.0463 \pm 0.0024$ , respectively. The energy density parameter is defined by  $\Omega_i \equiv \rho_i/\rho_c$ , where  $\rho_i$  is the density of species  $i = m$  and  $b$  and  $\rho_c \equiv 3H_0^2/(8\pi G)$  is the critical density. The present temperature of CBR is  $T_{\gamma 0} = 2.7255$  K [63]. The primordial abundances of hydrogen, helium, and lithium are from calculation of SBBN model [64] with the mean value of baryon density parameter  $\Omega_b$  described above, and the neutron lifetime  $878.5 \pm 0.7_{\text{stat}} \pm 0.3_{\text{sys}}$  s [65]: mass fractions of hydrogen and helium are  $X = 0.753$  and  $Y = 0.247$ , respectively, and the number ratio of lithium to hydrogen is  $\text{Li}/\text{H} = 5.2 \times 10^{-10}$ .

- redshift ( $z$ ) vs. time ( $t$ ) relation

$$a(t) = \frac{1}{1+z(t)} = \left( \frac{\Omega_m}{1-\Omega_m} \right)^{1/3} \left[ \sinh \left( \frac{\sqrt{3(1-\Omega_m)}}{2} H_0 t \right) \right]^{2/3}, \quad (34)$$

$$t = \frac{2H_0^{-1}}{\sqrt{3(1-\Omega_m)}} \sinh^{-1} \left[ \left( \frac{1}{1+z} \right)^{3/2} \left( \frac{1-\Omega_m}{\Omega_m} \right)^{1/2} \right], \quad (35)$$

where  $a(t)$  is the scale factor of the universe.

- baryon density



$$\begin{aligned}
\rho_b &= \rho_c \Omega_b (1+z)^3 (1+\delta) \\
&= 1.27 \times 10^{-26} \text{ g cm}^{-3} \left( \frac{h}{0.700} \right)^2 \left( \frac{\Omega_b}{0.0463} \right) \left( \frac{1+z}{17.5} \right)^3 \left( \frac{1+\delta}{5.55} \right),
\end{aligned} \tag{36}$$

where  $h \equiv H_0/(100 \text{ km s}^{-1} \text{ Mpc}^{-1})$  is the reduced Hubble constant, and  $1+\delta = \rho_m/\bar{\rho}_m$  is the density normalized to the universal average value  $\bar{\rho}_m$ . It has been assumed that the baryon density is proportional to the matter density.

- hydrogen number density

$$\begin{aligned}
n_H &\cong n_b X = \frac{\rho_b}{m_b} X \\
&= 5.69 \times 10^{-3} \text{ cm}^{-3} \left( \frac{h}{0.700} \right)^2 \left( \frac{\Omega_b}{0.0463} \right) \left( \frac{1+z}{17.5} \right)^3 \left( \frac{X}{0.75} \right) \left( \frac{1+\delta}{5.55} \right),
\end{aligned} \tag{37}$$

where  $n_b$  is the total baryon density, and  $m_b = 0.938 \text{ GeV}$  is the baryon mass.

- matter density

$$\begin{aligned}
\rho_m &= \rho_c \Omega_m (1+z)^3 (1+\delta) \\
&= 7.64 \times 10^{-26} \text{ g cm}^{-3} \left( \frac{h}{0.700} \right)^2 \left( \frac{\Omega_m}{0.279} \right) \left( \frac{1+z}{17.5} \right)^3 \left( \frac{1+\delta}{5.55} \right).
\end{aligned} \tag{38}$$

- spherical collapse model

The mass of the structure is  $M_{\text{str}} = 10^6 M_\odot$ . The collapse of the structure finishes at the redshift  $z_{\text{col}} = 10$ , or the cosmic time  $t_{\text{col}} = 0.483 \text{ Gyr}$ . The turnaround then occurs at  $z_{\text{tur}} = 16.5$ ,  $t_{\text{tur}} = t_{\text{col}}/2 = 0.242 \text{ Gyr}$ . The model structure is assumed to be a uniform density sphere with the radius at turnaround of

$$L = 597 \text{ pc} \left( \frac{M_{\text{str}}}{10^6 M_\odot} \right)^{1/3} \left( \frac{h}{0.700} \right)^{-2/3} \left( \frac{\Omega_m}{0.279} \right)^{-1/3} \left( \frac{1+z_{\text{tur}}}{17.5} \right)^{-1}, \tag{39}$$

which derives from  $M_{\text{str}} = (4\pi L^3/3)\rho_m(1+\delta)$  with density contrast  $1+\delta = 9\pi^2/16$  at turnaround. The comoving length scale is  $L_0 = (1+z_{\text{tur}})L = 10.4 \text{ kpc}$ .

The parameter  $A_G$  specifies the distance from the structure center. Choosing the  $A_G$  value as  $2A_G = L$  at the edge of the structure at turnaround, the  $B_G$  value is fixed to be

$$\begin{aligned}
B_G &= \sqrt{\frac{A_G^3}{GM_{\text{str}}}} = \sqrt{\frac{1}{6\pi^3 G \rho_m}} \\
&= 76.7 \text{ Myr} \left( \frac{h}{0.700} \right)^{-1} \left( \frac{\Omega_m}{0.279} \right)^{-1/2} \left( \frac{1+z_{\text{tur}}}{17.5} \right)^{-3/2}.
\end{aligned} \tag{40}$$

- magnetic field in the background universe

$$\begin{aligned}
B_z(z) &\sim B_{z0}(1+z)^2 \\
&= 3.06 \times 10^{-8} \text{ G} \left( \frac{B_{z0}}{10^{-10} \text{ G}} \right) \left( \frac{1+z}{17.5} \right)^2,
\end{aligned} \tag{41}$$

where  $B_{z0}$  is the  $z$ -component of the field value measured at present age, i.e., redshift  $z = 0$ .

- Larmor frequency of ion

$$\begin{aligned}\Omega_i &= \frac{Z_i e B}{m_i} \\ &= 28.4 Z_i \text{ yr}^{-1} \left( \frac{B}{10^{-10} \text{ G}} \right) \left( \frac{m_i}{1 \text{ GeV}} \right)^{-1},\end{aligned}\quad (42)$$

where  $Z_i$  is the charge number of ion  $i$ .

- gyration radius of ion

$$\begin{aligned}R_{i,g} &= \frac{m_i v_{i\perp}}{Z_i e B} = \frac{v_{i\perp}}{\Omega_i} \\ &= 1.08 Z_i^{-1} \times 10^{-8} \text{ pc} \left( \frac{v_{i\perp}}{10^{-6}} \right) \left( \frac{B}{10^{-10} \text{ G}} \right)^{-1} \left( \frac{m_i}{1 \text{ GeV}} \right),\end{aligned}\quad (43)$$

where  $v_{i\perp}$  is the velocity of  $i$  in the direction perpendicular to the magnetic field.

- cosmic recession velocity

$$\begin{aligned}v(r_p, z) &= H(z) r_p \\ &\sim \left[ H_0 \Omega_m^{1/2} (1+z)^{3/2} \right] r_p \\ &= 1.61 \text{ km s}^{-1} \left( \frac{h}{0.700} \right) \left( \frac{\Omega_m}{0.279} \right)^{1/2} \left( \frac{1+z}{17.5} \right)^{3/2} \left( \frac{r_p}{596 \text{ pc}} \right),\end{aligned}\quad (44)$$

where  $r_p(z)$  is the radius in a polar coordinate at redshift  $z$ , and the matter dominated universe was assumed for the Hubble expansion rate at  $z \gtrsim 10$ .

- gas temperature

$$T(z) = 22 \text{ K} \left( \frac{1+z}{17.5} \right)^2 \left( \frac{1+\delta}{5.55} \right)^{2/3}, \quad (45)$$

where the amplitude is taken from the calculation in Ref. [53].

- thermal average velocity of ion

$$\begin{aligned}v_{i,\text{th}} &= \sqrt{\frac{8T}{\pi m_i}} \\ &= 2.20 \times 10^{-6} \left( \frac{T}{22 \text{ K}} \right)^{1/2} \left( \frac{m_i}{1 \text{ GeV}} \right)^{-1/2}.\end{aligned}\quad (46)$$

- momentum transfer cross section of  $p+\text{H}$  at the relative velocity  $v_{\text{rel}} = 1.61 \text{ km s}^{-1}$

$$\sigma_{pn} = 1.4 \times 10^{-14} \text{ cm}^2. \quad (47)$$

- momentum transfer cross section of  ${}^7\text{Li}^++\text{H}$  at  $v_{\text{rel}} = 1.61 \text{ km s}^{-1}$

$$\sigma_{7n} = 1.3 \times 10^{-14} \text{ cm}^2. \quad (48)$$

- elastic scattering cross section of  $e+H$  at  $v_{\text{rel}} = 1.61 \text{ km s}^{-1}$

We approximately take the elastic scattering cross section [66]:

$$\begin{aligned}\sigma_{\text{en}} &\approx \sigma_{\text{en,el}} = 41\pi a_0^2 \\ &= 3.6 \times 10^{-15} \text{ cm}^2,\end{aligned}\tag{49}$$

where  $a_0 = 5.29 \times 10^{-9} \text{ cm}$  is the Bohr radius. The center of mass energy corresponding to  $v_{\text{rel}} = 1.61 \text{ km s}^{-1}$  is  $7.37 \text{ } \mu\text{eV}$ . The recession velocity is smaller than the electron thermal velocity,  $v_{e,\text{th}} = 29.1 \text{ km s}^{-1} (T/22 \text{ K})^{1/2}$  [Eq. (46)]. The thermal velocity is, therefore, appropriate for the relative velocity.

- Thomson scattering cross section

$$\begin{aligned}\sigma_{e\gamma} &= \frac{8\pi e^4}{3m_e^2} \\ &= 6.65 \times 10^{-25} \text{ cm}^2.\end{aligned}\tag{50}$$

Thomson scattering between electron and CBR is neglected since it does not occur so frequently, and its momentum transfer is negligible. The momentum transfer rate of electron, i.e.,  $n_\gamma \sigma_{e\gamma}$ , multiplied by the fractional change in electron momentum at one scattering  $\sim \mathcal{O}(T_\gamma/m_e)$ , is much smaller than that of the  $e+H$  scattering.

- momentum transfer rate of charged particles through the scattering with hydrogen

$$\begin{aligned}\tau_{\text{in}}^{-1} &= n_{\text{H}} (\sigma v)_{\text{in}} \\ &= 0.180 \text{ kyr}^{-1} \left( \frac{n_{\text{H}}}{5.69 \times 10^{-3} \text{ cm}^{-3}} \right) \left[ \frac{(\sigma v)_{\text{in}}}{10^{-9} \text{ cm}^3 \text{ s}^{-1}} \right],\end{aligned}\tag{51}$$

where  $(\sigma v)_{ij}$  is the cross section  $\sigma$  times velocity  $v$  in the reaction of  $i+j$ . In the equation, we have assumed that the reaction of  $i$  with neutral matter is dominated by that of  $i+H$ , and neglected reactions with other neutral atoms. The velocity is given by the larger of the hydrodynamic velocity difference,  $|\mathbf{v}_i - \mathbf{v}_j|$ , and the thermal mean velocity

$$v_{ij,\text{th}} = \sqrt{\frac{8T}{\pi\mu_{ij}}},\tag{52}$$

where  $\mu_{ij}$  is the reduced mass of the  $i + j$  system.

- friction parameter

A parameter representing the effect of the friction on a species  $i$  from a species  $j$  is defined as

$$\alpha_{ij} = \frac{m_i}{e\tau_{ij}}.\tag{53}$$

- energy loss rate via the Coulomb scattering

When the velocity of incident electron measured in the rest frame of ion  $j$ , i.e.,  $w$ , is much smaller than the root mean square velocity of target ion particle, the slowing-down time (the inverse of the energy loss rate) of electron via the scattering with ion is given [67] by

$$\tau_{ej} = \frac{3}{4\sqrt{2\pi}} \frac{m_e \mu_{ej} T^{3/2}}{e^4 m_j^{3/2} n_j \ln \Lambda},\tag{54}$$

where  $\mu_{ej} \sim m_e$  is the reduced mass of the  $e + j$  system. The quantity  $\ln \Lambda$  is related to the cutoff scale of scattering length, and is given by

$$\begin{aligned}\ln \Lambda &\equiv \ln \overline{h/p_0} = \ln \left[ \frac{3}{2e^3} \left( \frac{T^3}{\pi n_e} \right)^{1/2} \right] \\ &= 21.5 + \frac{3}{2} \ln \left( \frac{T}{22 \text{ K}} \right) - \frac{1}{2} \ln \left( \frac{n_{\text{H}}}{5.69 \times 10^{-3} \text{ cm}^{-3}} \right) - \frac{1}{2} \ln \left( \frac{\chi_{\text{H}^+}}{6.52 \times 10^{-5}} \right),\end{aligned}\tag{55}$$

where  $h$  is the Debye shielding distance,  $p_0$  is the impact parameter at a scattering through which an electron is deflected by the angle of  $\pi/2$ , and  $\chi_{\text{H}^+} = n_{\text{H}^+}/n_{\text{H}}$  is the ionization degree of hydrogen.

The energy loss rate is then given by

$$\tau_{ej}^{-1} = 2.21 \times 10^{-2} \text{ s}^{-1} \left( \frac{T}{22 \text{ K}} \right)^{-3/2} \left( \frac{m_j}{m_p} \right)^{3/2} \left( \frac{n_{\text{H}}}{5.69 \times 10^{-3} \text{ cm}^{-3}} \right) \left( \frac{\chi_{\text{H}^+}}{6.52 \times 10^{-5}} \right) \left( \frac{\ln \Lambda}{21.5} \right). \quad (56)$$

The parameter  $\alpha_{ej}$  is given by

$$\alpha_{ej} \equiv \frac{m_e}{e\tau_{ej}} = \frac{4\sqrt{2\pi} e^3 m_j^{3/2} Z_j^2 n_j \ln \Lambda}{3 \mu_{ej} T^{3/2}}. \quad (57)$$

We use the Newton's law of action and reaction [48], i.e.,

$$\frac{\rho_i}{\tau_{ij}} = \frac{\rho_j}{\tau_{ji}}. \quad (58)$$

A relation then holds in the case of  $n_p = n_e$ :

$$\alpha_{pe} = \alpha_{ep}. \quad (59)$$

The parameter  $\alpha_{ep} = \alpha_{pe}$  is given [Eq. (57)] by

$$\alpha_{ep} = 1.26 \times 10^{-9} \text{ G} \left( \frac{T}{22 \text{ K}} \right)^{-3/2} \left( \frac{n_{\text{H}}}{5.69 \times 10^{-3} \text{ cm}^{-3}} \right) \left( \frac{\chi_{\text{H}^+}}{6.52 \times 10^{-5}} \right) \left( \frac{\ln \Lambda}{21.5} \right). \quad (60)$$

We use Eq. (58) for the  $e+{}^7\text{Li}^+$  system, and derive

$$\begin{aligned} \alpha_{7e} &= \alpha_{e7} \frac{n_e}{n_7} = \frac{4\sqrt{2\pi} e^3 m_7^{3/2} n_p \ln \Lambda}{3 \mu_{e7} T^{3/2}} \\ &\sim \left( \frac{m_7}{m_p} \right)^{3/2} \alpha_{ep}. \end{aligned} \quad (61)$$

We also use Eq. (58) for the  $p+{}^7\text{Li}^+$  system, and derive

$$\begin{aligned} \alpha_{7p} &= \alpha_{p7} \frac{n_p}{n_7} = \frac{4\sqrt{2\pi} e^3 m_7^{3/2} n_p \ln \Lambda}{3 \mu_{p7} T^{3/2}} \\ &= \alpha_{7e} \frac{\mu_{e7}}{\mu_{p7}} \sim \frac{8m_e}{7m_p} \alpha_{7e} \ll \alpha_{7e}. \end{aligned} \quad (62)$$

The friction from the  $p+{}^7\text{Li}^+$  scattering is then neglected.

- escape fraction of ion

The fraction of an ion escaping through outer boundary of the structure during the structure formation is estimated as

$$F_{i,\text{esc}}(t) = \frac{\Delta M_i(t)}{M_i} = \frac{\int_{t_i}^t \dot{M}_i(t') dt'}{M_i}, \quad (63)$$

where  $M_i$  is the total mass of ion  $i$  initially contained in the structure before the contraction,  $\Delta M_i(t)$  is the total mass of ion  $i$  which escaped from the structure by time  $t$ , and  $t_i$  is the initial time which should be larger than the time of the primordial nucleosynthesis  $\sim 200$  s. Under the assumption of the spherical symmetry in infall of neutral hydrogen and the axial symmetry in the ion infall, the mass loss rate is given by

$$\dot{M}_i(t) = 2\pi r_{\text{str}}^2(t) \int_0^\pi \sin \theta d\theta \rho_i(t, r_{\text{str}}(t), \theta) v_{i,\text{esc}}(t, r_{\text{str}}(t), \theta), \quad (64)$$

where  $r_{\text{str}}(t)$  is the radius of the structure in a polar coordinate at time  $t$ ,  $\theta = \tan^{-1}(r/z)$  is the angle between the position vector and the symmetrical  $z$  axis, and  $\rho_i(t, r_{\text{str}}(t), \theta)$  is the density at position  $(r_{\text{str}}(t), \theta)$  at time  $t$ . The variable  $v_{i,\text{esc}}(t, r_{\text{str}}(t), \theta)$  is the escape velocity defined by

$$\begin{aligned} v_{i,\text{esc}}(t, r_{\text{str}}(t), \theta) &= (\mathbf{v}_i - \mathbf{v}_n) \cdot \hat{r} \\ &= \sin \theta [v_{ir}(t, r_{\text{str}}(t), \theta) - v_{nr}(t, r_{\text{str}}(t), \theta)] \\ &\quad + \cos \theta [v_{iz}(t, r_{\text{str}}(t), \theta) - v_{nz}(t, r_{\text{str}}(t), \theta)], \end{aligned} \quad (65)$$

where  $\hat{r}$  is the unit vector with the direction of the position vector  $\mathbf{r}$ .

When we assume that the density in the structure is homogeneous, the mass loss rate reduces to

$$\dot{M}_i(t) = \frac{3M_i}{2r_{\text{str}}(t)} \int_0^\pi \sin \theta d\theta v_{i,\text{esc}}(t, r_{\text{str}}(t), \theta). \quad (66)$$

The escape fraction of ion  $i$  is then given by

$$\begin{aligned} F_{i,\text{esc}}(t) &= \frac{3}{2} \int_{t_i}^t dt' \frac{1}{r_{\text{str}}(t')} \int_0^\pi \sin \theta d\theta v_{i,\text{esc}}(t', r_{\text{str}}(t'), \theta) \\ &= 2 \int_{\ln t_i}^{\ln t} \frac{\langle v_{i,\text{esc}}(t', r_{\text{str}}(t')) \rangle_\mu}{H(t') r_{\text{str}}(t')} d \ln t', \end{aligned} \quad (67)$$

where  $\langle v_{i,\text{esc}}(t', r_{\text{str}}(t')) \rangle_\mu \equiv (1/2) \int_{-1}^1 d\mu v_{i,\text{esc}}(t', r_{\text{str}}(t'), \cos^{-1} \mu)$  is the average value of the escape velocity. The recession velocity at the structure edge,  $r_p = r_{\text{str}}(t)$ , is  $H(t)r_{\text{str}}(t)$ . The integration in the expression of  $F_{i,\text{esc}}(t)$  is then dominated by the epoch when the escape velocity is significant fraction of the recession velocity.

#### IV. RESULT

We assume two cases of magnetic field amplitudes,  $B_{z0} = 5 \times 10^{-10}$  G (Case 1) and  $5 \times 10^{-11}$  G (Case 2). The former value is enough large so that charged chemical species escape from a gravitational collapse with neutral hydrogen, while the latter is not. The mass of the structure is  $10^6 M_\odot$  in the both cases. The electric current density  $\mathbf{j}$  is determined from rotation of the magnetic field through the Ampere's equation [Eq. (15)]. The friction of infalling neutral hydrogen changes the radial velocities of charged species through a balance between the friction and Lorentz forces.

The mass of the structure is chosen for the following reason. The chemical separation of charged and neutral species proceeds during the enhancement of matter density associated with the gravitational collapse of structures. In the  $\Lambda$ CDM cosmological model, small structures form earlier. Larger structures such as galaxies form through collisions and mergers of smaller structures. If we only consider structures collapsing during the redshift of  $z = 30 - 10$  in which baryonic matter can form astrophysical objects, structure masses should be larger than  $\sim 10^6 - 10^8 M_\odot$  [68]. Significant fractions of baryonic matters in large structures which are observed today, therefore, have experience that they enhanced their densities at gravitational contractions of small structures with nearly the minimum masses. We then assume a small structure with mass  $10^6 M_\odot$  as a first structure. Although the merger is a dominant cause of the formation of large structures, a part of baryonic matter is expected to have flown into the structures along filament structures [69]. It is, therefore, not to say that almost all material experienced the density enhancement at gravitational collapses of near-spherical structures.

In this section, we show results of time evolutions for average densities of chemical species, spatial distributions of the densities and azimuthal magnetic field. Results of other physical variables are described in Appendix B.

##### A. Average densities vs. time

Figure 2 shows densities of hydrogen (open circles), proton and  ${}^7\text{Li}^+$  for Case 1 (open diamonds) and Case 2 (filled triangles) averaged over the structure volume as a function of cosmic time  $t$ . The densities are normalized as  $\rho_i / (A_i \bar{\chi}_i)$ , where  $A_i$  is the mass number of  $i$  and  $\bar{\chi}_i \equiv \overline{(n_i/n_{\text{H}})}$  is the initial cosmic average value for the number ratio of  $i$  to hydrogen. Solid lines show analytical curves of hydrogen densities in the structure (upper line) and IGM (lower).

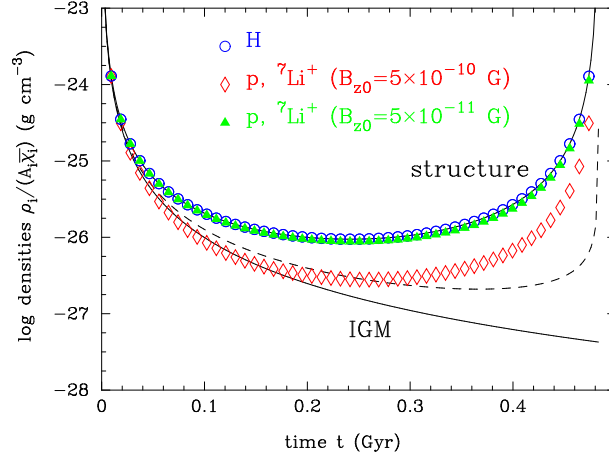


FIG. 2: Calculated average densities of hydrogen (open circles), proton and  ${}^7\text{Li}^+$  for Case 1 (open diamonds) and Case 2 (filled triangles) in the structure as a function of cosmic time  $t$ . The densities are normalized by the factor of nuclear mass number  $A_i$  times the initial cosmic average value for the number ratio of  $i$  and hydrogen  $\bar{\chi}_i$ . Solid lines show analytical curves of hydrogen densities in the structure (upper line) and IGM (lower). It was assumed that inside the structure, the density is determined by the gravitational free fall of matter, and that outside the density is given by the cosmic average density. The dashed line shows an analytical curve for charged species such as proton and  ${}^7\text{Li}^+$  based on the following assumption: The species can collapse gravitationally along the axis of magnetic field, but expands across the field exactly following the cosmic average expansion.

They are calculated based on the following assumption: Outside the structure, the density is given by cosmic average density:

$$\begin{aligned} \rho_{\text{H}}^{\text{O}}(t) &= \bar{\rho}_{\text{H}}(t) \\ &= \rho_{\text{H}}^{\text{O}}(t_i) \left( \frac{1+z}{1+z_i} \right)^3, \end{aligned} \quad (68)$$

where  $z$  and  $z_i$  are redshifts corresponding to time  $t$  and  $t_i$ , respectively. Inside the structure, on the other hand, the density is given by

$$\begin{aligned} \rho_{\text{H}}^{\text{I}}(t) &= \rho_{\text{b}}(t_i) X \left[ \frac{r(t_i)}{r(t)} \right]^3 = \frac{3}{4\pi} \frac{M_{\text{str}}}{A_{\text{G}}^3 (1 - \cos\theta)^3} \left( \frac{\Omega_{\text{b}}}{\Omega_{\text{m}}} \right) X \\ &= 7.57 \times 10^{-26} (1 - \cos\theta)^{-3} \text{ g cm}^{-3} \left( \frac{M_{\text{str}}}{10^6 M_{\odot}} \right) \left( \frac{A_{\text{G}}}{298 \text{ pc}} \right)^{-3} \left( \frac{\Omega_{\text{b}}}{0.0463} \right) \left( \frac{\Omega_{\text{m}}}{0.279} \right)^{-1} \left( \frac{X}{0.75} \right). \end{aligned} \quad (69)$$

When effects of magnetic field are small, curves of  $\text{H}^+$  and  ${}^7\text{Li}^+$  should be nearly the same as that of hydrogen. The dashed line shows an analytical curve for charged species such as proton and  ${}^7\text{Li}^+$  based on the following assumption: The species can collapse gravitationally along the axis of magnetic field ( $z$ -axis), and just expands across the field at the same velocity as the cosmic average expansion. In this case, its density evolves as

$$\rho_i^{\text{I}}(t) = \rho_i^{\text{I}}(t_i) \frac{r(t_i)}{r(t)} \left[ \frac{1+z}{1+z_i} \right]^2 = A_i \bar{\chi}_i [\rho_{\text{H}}^{\text{I}}(t)]^{1/3} [\rho_{\text{H}}^{\text{O}}(t)]^{2/3}, \quad (70)$$

where it was assumed that hydrogen densities inside and outside the structure, i.e.,  $\rho_{\text{H}}^{\text{I}}(t)$  and  $\rho_{\text{H}}^{\text{O}}(t)$ , respectively, are almost equal at initial time  $t_i (\ll t)$  which is taken to be enough small.

In Case 1, the dilution of charged species in the structure proceeds at the intermediate phase with low densities. This dilution can be observed as the ratio between the normalized densities of  $p$  (and  ${}^7\text{Li}$ ) and hydrogen which reduces when the density becomes low around the turnaround. In the early and late phases of high densities, dilutions do not proceed effectively since the motions of charged and neutral species are strongly coupled in high density environments. Eventually, the  ${}^7\text{Li}$  ion is diluted in the structure by a factor of  $\sim 4$  in the end of the calculation. This dilution history is qualitatively applied to Case 2. The dilution factor is, however, much smaller in Case 2.

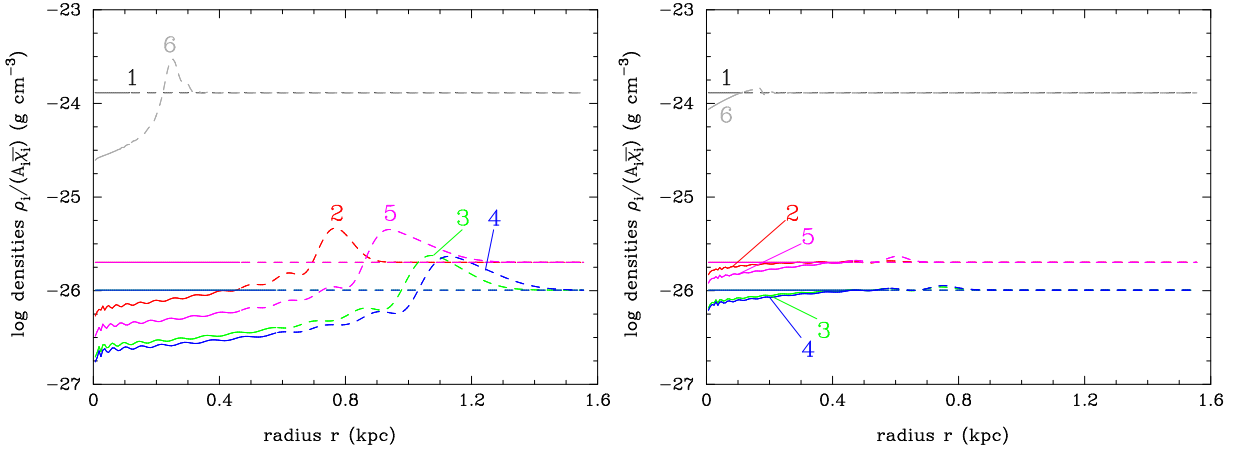


FIG. 3: Normalized densities of hydrogen (straight lines), proton and  ${}^7\text{Li}^+$  (curves) as a function of radius from the structure center for Case 1 (left panel) and Case 2 (right panel) at  $t=9.29$  Myr (1), 102 Myr (2), 195 Myr (3), 288 Myr (4), 381 Myr (5), and 474 Myr (6). Solid and dashed lines correspond to the regions inside and outside the structure, respectively.

### B. Chemical separation

Figure 3 shows normalized densities of hydrogen (straight lines), proton and  ${}^7\text{Li}^+$  (curves) as a function of radius from the structure center for Case 1 (left panel) and Case 2 (right panel). Density distributions are drawn for six different times:  $t=9.29$  Myr (denoted by number 1), 102 Myr (2), 195 Myr (3), 288 Myr (4), 381 Myr (5), and 474 Myr (6). Note that structure sizes or densities of neutral hydrogen are the same at times 1 and 6, 2 and 5, and 3 and 4, respectively, although times 1-3 are in an expanding phase, and times 4-6 are in a collapsing phase. Solid and dashed lines correspond to the regions inside and outside of the structure, respectively. The initial gradient of  $B_z$  causes an expansion of the charged-species fluid. Since the  $B_z$  value is large at a small radius, the expansion is fast in the region of small  $r$ . Accordingly the magnetic field amplitude and its gradient rapidly decrease in the inner region of small  $r$ . Since the gradient of  $B_z$  is not assumed in the outer region of large  $r$ , movements of charged particles do not occur in the outer region. Then, high density shells forms at the boundaries between the inner and outer regions as seen in this figure as bumps. The curves for the densities of charged species have oscillatory structures as well as the bumps caused by the assumed initial condition. The dilution of charged species inside the structure is more efficient in Case 1 than in Case 2 because of the stronger magnetic field.

### C. Magnetic field

Figure 4 shows the magnetic field ( $z$ -component) as a function of radius for Case 1 (left panel) and Case 2 (right panel). Solid and dashed lines correspond to values inside and outside the structure, respectively. Additionally to the effect of expansion and collapse of neutral hydrogen, a weakening of magnetic field is observed in the small  $r$  region. This dilution is caused by outward movements of charged species (Fig. 3). It is seen that a decrease in  $B_z$  in the small  $r$  region caused by outgoing charged species is more significant in Case 1 than in Case 2.

## V. MAGNETIC FIELD AMPLITUDE

In preceding sections, a magnetic field generation is neglected. The generation, however, proceeds through a drift current creation in the structure, although its effect is insignificant which is explained as follows.

The time evolution of magnetic field in a structure is described [29] as

$$\left| \frac{dB}{dt} \right| = \frac{1}{4\pi\sigma_e} |\nabla^2 B| \approx \frac{B}{4\pi\sigma_e L_B^2}, \quad (71)$$

where

$$\sigma_e = \frac{n_e e^2 \tau_{ep}}{m_e} \quad (72)$$



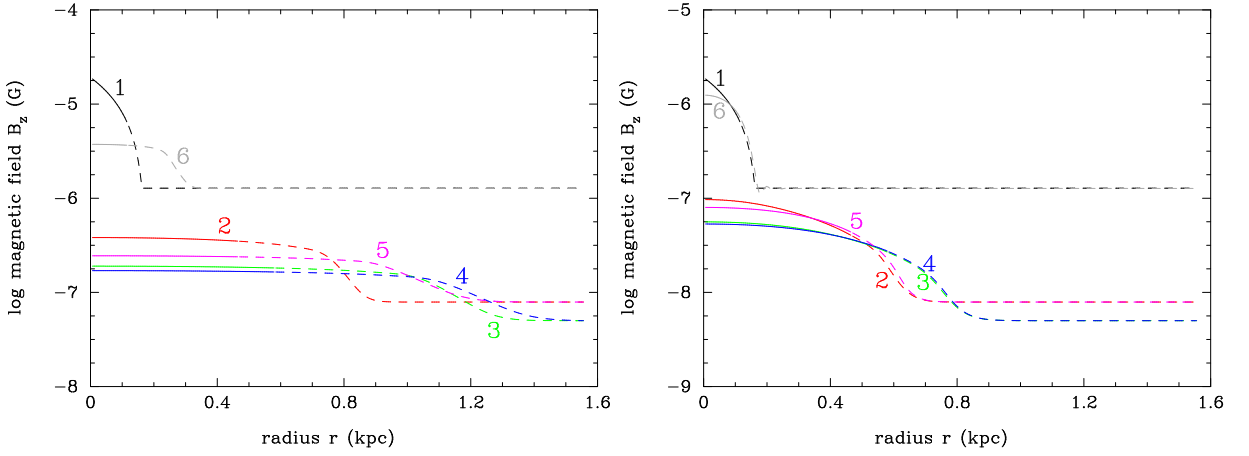


FIG. 4: Magnetic field ( $z$ -component) as a function of radius for Case 1 (left panel) and Case 2 (right panel) at  $t=9.29$  Myr (1), 102 Myr (2), 195 Myr (3), 288 Myr (4), 381 Myr (5), and 474 Myr (6). Solid and dashed lines correspond to values inside and outside the structure, respectively.

is the electron conductivity [26]. The diffusion time of the magnetic field on a length scale  $L_B$  during the early structure formation is then given by

$$\begin{aligned}\tau_{\text{diff}}(L_B) &= 4\pi\sigma_e L_B^2 \\ &= 6.39 \times 10^{18} \text{ yr} \left(\frac{T}{22 \text{ K}}\right)^{3/2} \left(\frac{\ln \Lambda}{21.5}\right)^{-1} \left(\frac{L_B}{597 \text{ pc}}\right)^2.\end{aligned}\quad (73)$$

Thus, large inductances of large astrophysical objects result in very long diffusion times. The generation of magnetic field in the cosmological time scale is, therefore, impossible. The self-inductance of astrophysical objects with length scale  $L_B$  is given by  $L_{\text{ind}}(L_B) \sim \mu_m L_B$ , where  $\mu_m$  is the magnetic permeability. When some electromotive force is created in the structure, the electric current is produced at an approximately constant production rate which is inversely proportional to the inductance. The magnetic energy  $W$  stored in a coil, that is the structure itself in the present case, is proportional to the electric current squared,  $W = L_{\text{ind}}(L_B)I^2/2 \sim \mu_m L_B I^2$ . The magnetic energy per volume,  $L_B^3$ , is then proportional to the length scale squared:  $W/L_B^3 \sim \mu_m L_B (jL_B^2)^2/L_B^3 \sim \mu_m j^2 L_B^2$ . The generation of magnetic field on a large scale of  $L_B$ , therefore, requires large amount of source energy density. For the reason above, the generation of magnetic field by an electric current associated with dynamical friction never proceeds effectively.

The Ampere's equation [Eq. (15)] gives the relation between an electric current density and a magnetic field as

$$j_\phi \sim \frac{B_z}{4\pi L_B} = 2.89 \times 10^{-13} \text{ cm}^{-2} \text{ s}^{-1} \left(\frac{B_z}{10^{-10} \text{ G}}\right) \left(\frac{L_B}{597 \text{ pc}}\right)^{-1}.\quad (74)$$

If a magnetic field and an electric current density existed from the beginning of the structure formation, and the Lorentz force is enough large to realize a separation between charged and neutral species, charged species possibly do not collapse gravitationally. The charged species, therefore, do not participate in structure formations. Although fluid motions of charged species are different from that of neutral species, scatterings between charged and neutral species efficiently transfer the kinetic energy of neutral species to charged species. The velocity difference between H and proton has typically been assumed to be the cosmological recession velocity in the present case [Eq. (44)]. This velocity corresponds to the proton temperature of  $T \sim m_p v_{\text{rel}}^2/6 = 52.3 \text{ K}$ . The scatterings then gradually increase the temperature of charged species as a function of time. Resultantly, it is expected that the friction time scale,  $\tau_{ej}$  [cf. Eq. (56)], increases.

The equilibrium amplitude of the magnetic field is then related with the velocity difference through Eqs. (14) and (74):

$$\begin{aligned}B_z &\sim \sqrt{4\pi L_B j_\phi B_z} \sim \sqrt{4\pi L_B e n_p (\alpha_{pn} + \alpha_{en}) (v_{pr} - v_{nr})} \\ &= 7.40 \times 10^{-8} \text{ G} \left(\frac{n_H}{5.69 \times 10^{-3} \text{ cm}^{-3}}\right) \left(\frac{\chi_{H^+}}{6.52 \times 10^{-5}}\right)^{1/2} \left(\frac{\Delta v_r}{1.61 \text{ km s}^{-1}}\right)^{1/2} \left(\frac{L_B}{597 \text{ pc}}\right)^{1/2}\end{aligned}$$

$$\times \left[ \frac{(\sigma v)_{pH}}{2.3 \times 10^{-9} \text{ cm}^3 \text{ s}^{-1}} \right]^{1/2}, \quad (75)$$

where  $\Delta v_r = v_{pr} - v_{nr}$  is the velocity difference. In the second line, we assumed typical physical values estimated at the gravitational turnaround  $z = z_{\text{tur}} = 16.5$  and the critical value of  $\Delta v_r$  given by the cosmological recession velocity at the turnaround [Eq. (44)]. The corresponding comoving magnetic field is  $B_{z0} = B_z(z_{\text{tur}})/(1 + z_{\text{tur}})^2 = 0.242 \text{ nG}$ . We note that the minimum amplitude of magnetic field which can support the charged species against the dynamical friction is larger if a larger structure is considered (Sec. VB).

If the time scale of field generation were shorter than the dynamical time of the system, an azimuthal electric current density is gradually induced by  $\mathbf{F} \times \mathbf{B}$  drifts leading to a generation of a poloidal magnetic field. Magnetic fields in astronomical objects can be related to electric currents existing in their interiors. In general, the fields are generated by electric currents which themselves are formed by motions of charged species,  $\mathbf{v}_i$ , in regions with finite magnetic fields. This process for an amplification of magnetic field is called self-exciting dynamo, and is thought to operate in the Sun, Earth, other planets, interstellar clouds, and Galaxy [71]. The self-exciting dynamo effectively operates if a primary field exists initially, and has its origin different from the dynamo. One of requirements for a self-exciting dynamo is an enough energy release inside the object to energize the dynamo [72].

### A. Two stream instability

A relative motion of an electron fluid through an ion fluid can cause a micro-instability [73]. If the relative velocity exceeds a critical value, a turbulence is triggered. In the case that the temperatures of electron and proton are equal, the critical values of relative velocity is  $v_{\text{rel}} = \mathcal{F}C_e$ , where  $\mathcal{F} \approx 0.604$  is a factor fixed for the maximum growth rate of instability, and  $C_e \equiv (T_e/m_e)^{1/2}$  is a measure for thermal speed of electron.

However, the relative velocity is much smaller than the electron thermal velocity even when the azimuthal electric current density is so high that the radial velocity difference of proton and hydrogen is equal to the cosmic recession velocity at the turnaround. Then, the instability does not occur. The relative velocity is given by

$$\begin{aligned} v_{\text{rel}} &= v_{p\phi} - v_{e\phi} \approx \frac{\alpha_{pn}}{B_z} HL \\ &= 5.39 \times 10^{-4} \text{ cm s}^{-1} \left( \frac{\chi_{H^+}}{6.52 \times 10^{-5}} \right)^{-1/2} \left( \frac{H}{2.70 \times 10^3 \text{ km s}^{-1} \text{ Mpc}^{-1}} \right)^{1/2} \left[ \frac{(\sigma v)_{pH}}{2.3 \times 10^{-9} \text{ cm}^3 \text{ s}^{-1}} \right]^{1/2} \\ &\quad \times \left( \frac{L}{L_B} \right)^{1/2}, \end{aligned} \quad (76)$$

where Eqs. (51), (53), (75), (A7), and (A17) were used. On the other hand, the  $C_e$  value is given by

$$\begin{aligned} C_e &\equiv \sqrt{T_e/m_e} \\ &= 1.83 \times 10^6 \text{ cm s}^{-1} \left( \frac{1+z}{17.5} \right) \left( \frac{1+\delta}{5.55} \right)^{1/3}. \end{aligned} \quad (77)$$

### B. Magnetic field generation in molecular cloud

We roughly check an amplitude of magnetic field generated through a drift current in MCs. For this purpose, we take physical quantities near the surface of MCs in Model A of Ref. [49]:  $n_H \sim 2.6 \times 10^3 \text{ cm}^{-3}$ ,  $\chi_{H^+} \sim 10^{-10}$ ,  $L \sim 4.3 \text{ pc}$ ,  $B \sim 35.3 \text{ } \mu\text{G}$ ,  $|v_{nr}| \sim 1.9 \times 10^3 \text{ cm s}^{-1}$ ,  $\sigma_{pn}(\Delta v_r \sim 10^3 \text{ cm s}^{-1}) \sim 1.6 \times 10^{-13} \text{ cm}^2$ . The  $\alpha_{pn}$  value [Eqs. (51) and (53)] is then estimated to be

$$\alpha_{pn} = 5.87 \times 10^{-12} \text{ G} \left( \frac{n_H}{10^3 \text{ cm}^{-3}} \right) \left[ \frac{(\sigma v)_{pH}}{3.1 \times 10^{-10} \text{ cm}^3 \text{ s}^{-1}} \right]. \quad (78)$$

The amplitude of generated field is then given [Eqs. (14) and (74)] by

$$\delta B_z \sim 4\pi j_\phi L_B = \frac{4\pi e n_p \alpha_{pn} \Delta v_r L_B}{B_z}$$

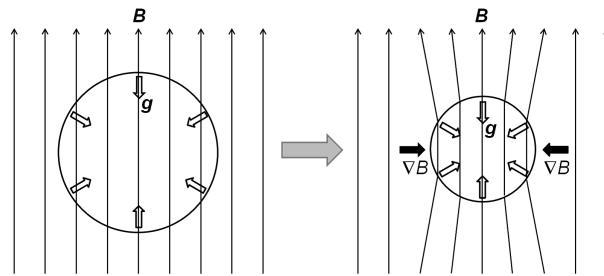


FIG. 5: Illustration of the creation of magnetic field gradient in the radial direction. The upper direction is defined as the  $z$ -axis, and open circles correspond to boundaries of a structure at an early epoch before the gravitational contraction (left part) and at a late epoch during the contraction (right part). Thin arrows show magnetic field lines, open thick arrows indicate directions of the gravity, and filled thick arrows indicate directions of the magnetic field gradient.

$$\begin{aligned}
 &= 3.64 \times 10^{-11} \text{ G} \left( \frac{n_{\text{H}}}{10^3 \text{ cm}^{-3}} \right)^2 \left( \frac{\chi_{\text{H}^+}}{10^{-10}} \right) \left[ \frac{(\sigma v)_{\text{pH}}}{3.1 \times 10^{-10} \text{ cm}^3 \text{ s}^{-1}} \right] \left( \frac{B_z}{10 \mu\text{G}} \right)^{-1} \left( \frac{\Delta v_r}{10^3 \text{ cm s}^{-1}} \right) \\
 &\quad \times \left( \frac{L_B}{1 \text{ pc}} \right). \tag{79}
 \end{aligned}$$

This is much smaller than the magnetic field initially assumed to exist in a MC,  $B_{\text{eq},c0} = 35.3 \mu\text{G}$ . The field generation, therefore, does not affect at all the total amplitude of magnetic field during the time evolution of the model MC.

## VI. GENERATION OF A MAGNETIC FIELD GRADIENT

In the present calculation, gradients of the magnetic field in the  $r$ -direction are assumed in the initial conditions. Practically, charged species of ions and electron totally move outward only in special configurations of magnetic fields as in the setting of this paper. A gradient of the magnetic field can, however, be generated through the gravitational collapse of a structure even if the initial magnetic field amplitude is coherent and homogeneous.

Figure 5 shows an illustration for the creation of magnetic field gradient in the  $r$ -direction. The upper direction on the plane of paper is defined as the  $z$ -axis, and open circles correspond to boundaries of a structure at an early epoch before the gravitational contraction (left part) and at a late epoch during the contraction (right part). Thin arrows show magnetic field lines, open thick arrows indicate directions of the gravity, and filled thick arrows indicate directions of the magnetic field gradient. The density of baryon inside the structure increases relative to that of outside as a function of time. Since field lines are initially frozen into the charged plasma, the  $B_z$  value increases inside the structure. A gradient of the magnetic field is then generated in the  $r$ -direction near the boundary (right part). Consequently, the Lorentz force is produced in the  $r$ -direction with its strength proportional to  $[(\nabla \times \mathbf{B}) \times \mathbf{B}]_r \sim -(\partial_r B_z) B_z$  [Eq. (20)].

## VII. PARAMETER REGION FOR CHEMICAL SEPARATION

### A. Scales of structure and magnetic domain

In the  $\Lambda$ CDM cosmological model, large structures such as galaxies and galactic clusters form through collisions and mergers of smaller structures. When we consider gravitational collapses of structures with scales smaller than that of Galaxy, effects of the magnetic field on motions of charged and neutral species are quantitatively different from that of larger structures. For example, the velocity difference of neutral and charged species at the time of turnaround, i.e.,  $H(z_{\text{tur}})r_p$ , needed for charged species to escape from gravitational collapse is smaller for smaller structures.

We note that the typical scale of magnetic domain in which the field direction is coherent should be larger than the system scale. If the scale of magnetic domain is smaller than the system scale, average radial velocities of charged species are roughly the same as that of neutral species although there are fluctuations in velocities caused by the magnetic field existing over small scales. We, therefore, have a constraint on the comoving  $L_{B0}$  value, i.e.,  $L_{B0} \geq L(1+z)$  [cf. Eq. (39)].

## B. Constraints

The condition for the gravitational collapse of neutral matter is that the gravitation [the first term in RHS of Eq. (19)] is larger than the Lorentz force (the second term). It is clear that magnetic fields on the scale larger than 600 pc with amplitude less than  $\sim 10^{-7}$  G do not affect the gravitational collapse of neutral atoms [Eqs. (22) and (23)]. When the amplitude and the spatial scale of magnetic field satisfy the condition, the gravitational collapse of neutral species can realize. Using Eqs. (22), (23), (36), and (38), the condition is derived:

$$\frac{B_z^2}{L_B} < 1.93 \times 10^{-14} \text{ G}^2 \text{ kpc}^{-1} \left( \frac{1+z_{\text{tur}}}{17.5} \right)^5 \left( \frac{h}{0.700} \right)^{10/3} \left( \frac{\Omega_b}{0.0463} \right) \left( \frac{\Omega_m}{0.279} \right)^{2/3} \left( \frac{M_{\text{str}}}{10^6 M_\odot} \right)^{1/3}. \quad (80)$$

The comoving value is related to the proper value by  $B_{z0}^2/L_{B0} = (1+z)^{-5} B_z^2/L_B$ . The condition on the comoving value is then given by

$$\frac{B_{z0}^2}{L_{B0}} < 1.18 \times 10^{-20} \text{ G}^2 \text{ kpc}^{-1} \left( \frac{h}{0.700} \right)^{10/3} \left( \frac{\Omega_b}{0.0463} \right) \left( \frac{\Omega_m}{0.279} \right)^{2/3} \left( \frac{M_{\text{str}}}{10^6 M_\odot} \right)^{1/3}. \quad (81)$$

This constraint is independent of the turnround redshift  $z_{\text{tur}}$ .

The condition for that charged species do not collapse gravitationally with neutral hydrogen is that the Lorentz force is larger than the friction of neutral hydrogen for the velocity difference given by the cosmic recession velocity at the turnround, i.e.,  $v_{pr} - v_{nr} > H(z_{\text{tur}})r_p$ . When the amplitude and scale of magnetic field satisfy the condition, the leaving of charged species in IGM can be typically realized. The friction on proton is the predominant friction working on the whole charged fluid in the radial direction, and the proton velocity is related to the velocity of neutral matter [Eq. (30)].

Using Eqs. (23), (37), (38), (39), and (44), the condition is derived:

$$\begin{aligned} \frac{B_z^2}{L_B} &> 1.53 \times 10^{-14} \text{ G}^2 \text{ kpc}^{-1} \left( \frac{1+z_{\text{tur}}}{17.5} \right)^{13/2} \left( \frac{h}{0.700} \right)^{13/3} \left( \frac{\Omega_b}{0.0463} \right)^2 \left( \frac{X}{0.75} \right)^2 \left( \frac{\Omega_m}{0.279} \right)^{1/6} \\ &\times \left( \frac{\chi_{\text{H}^+}}{6.52 \times 10^{-5}} \right) \left[ \frac{(\sigma v)_{p\text{H}}}{2.3 \times 10^{-9} \text{ cm}^3 \text{ s}^{-1}} \right] \left( \frac{M_{\text{str}}}{10^6 M_\odot} \right)^{1/3}. \end{aligned} \quad (82)$$

The condition on the comoving value is also given by

$$\begin{aligned} \frac{B_{z0}^2}{L_{B0}} &> 9.33 \times 10^{-21} \text{ G}^2 \text{ kpc}^{-1} \left( \frac{1+z_{\text{tur}}}{17.5} \right)^{3/2} \left( \frac{h}{0.700} \right)^{13/3} \left( \frac{\Omega_b}{0.0463} \right)^2 \left( \frac{X}{0.75} \right)^2 \left( \frac{\Omega_m}{0.279} \right)^{1/6} \\ &\times \left( \frac{\chi_{\text{H}^+}}{6.52 \times 10^{-5}} \right) \left[ \frac{(\sigma v)_{p\text{H}}}{2.3 \times 10^{-9} \text{ cm}^3 \text{ s}^{-1}} \right] \left( \frac{M_{\text{str}}}{10^6 M_\odot} \right)^{1/3}. \end{aligned} \quad (83)$$

Figure 6 shows constraints on the comoving Lorentz force  $B_{z0}^2/L_{B0}$  as a function of the turnround redshift  $z_{\text{tur}}$ . Solid lines correspond to lower limits from the condition that charged species do not contract with neutral hydrogen [Eq. (81)]. Dashed lines correspond to upper limits from the condition of the gravitational collapse of neutral hydrogen [Eq. (83)]. For respective constraints, lines are shown for three cases of the structure mass,  $M_{\text{str}} = 10^6$  (the lowest lines),  $10^9$  (the middle lines), and  $10^{12} M_\odot$  (the highest lines). For  $M_{\text{str}} = 10^6 M_\odot$ , we find a parameter region for a successful chemical separation with  $B_{z0}^2/L_{B0} \lesssim 10^{-20} \text{ G}^2 \text{ kpc}^{-1}$  in the redshift region of  $1+z_{\text{tur}} \lesssim 20$ . For  $M_{\text{str}} = 10^9 M_\odot$ , a similar interesting parameter region exists at  $B_{z0}^2/L_{B0} \lesssim 10^{-19} \text{ G}^2 \text{ kpc}^{-1}$  and  $1+z_{\text{tur}} \lesssim 7$ . For the most massive case of  $M_{\text{str}} = 10^{12} M_\odot$ , no region is found at relatively high redshifts of  $1+z_{\text{tur}} \sim 10$ . In this way, at gravitational collapses of heavier objects, it is more difficult to separate the motions of neutral and charged particles.

Figure 7 shows constraints on the comoving Lorentz force as a function of the structure mass  $M_{\text{str}}$ . Solid lines correspond to lower limits from the condition for the motion of charged species [Eq. (81)] for three cases of the turnround redshift,  $1+z_{\text{tur}} = 17.5$ , 25.4, and 33.3 (corresponding to the collapse redshift  $z_{\text{col}} = 10$ , 15, and 20, respectively). The dashed line shows the upper limit from the condition of the gravitational collapse of neutral hydrogen, which are independent of the turnround redshift [Eq. (83)]. It can be seen that the chemical separation is more difficult in structures which collapse earlier. We find the parameter region for the chemical separation at  $M_{\text{str}} \sim \mathcal{O}(10^6) M_\odot$  only for the latest collapse case of  $1+z_{\text{tur}} = 17.5$ .

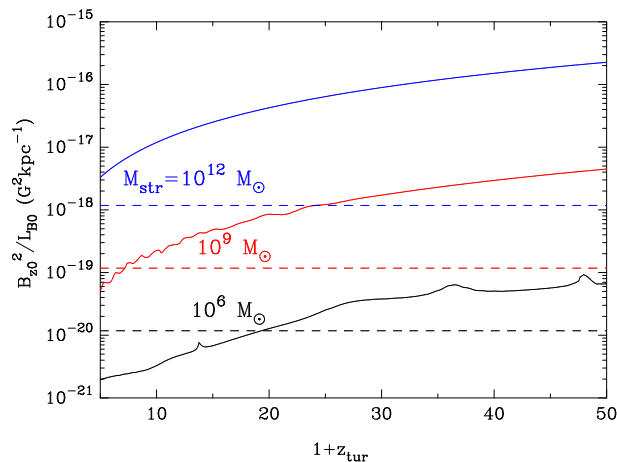


FIG. 6: Constraints on the comoving Lorentz force as a function of the turnround redshift. Solid lines show lower limits from the condition that charged species do not contract with neutral hydrogen. Dashed lines show upper limits from the condition of the gravitational collapse of neutral hydrogen. Lines are drawn for three cases of the structure mass,  $M_{\text{str}} = 10^6, 10^9, \text{ and } 10^{12} M_{\odot}$ .

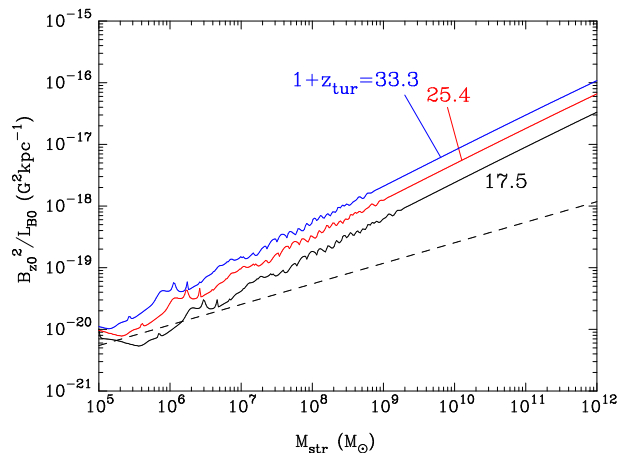


FIG. 7: Constraints on the comoving Lorentz force as a function of the structure mass. Solid lines show lower limits from the condition that charged species do not contract with neutral hydrogen. Lines are drawn for three cases of the turnround redshift,  $1 + z_{\text{tur}} = 17.5, 25.4, \text{ and } 33.3$  (corresponding to the collapse redshift  $z_{\text{col}} = 10, 15, \text{ and } 20$ , respectively). The dashed line shows the upper limit from the condition of the gravitational collapse of neutral hydrogen independently of the turnround redshift.

## VIII. DISCUSSION

### A. Later epoch of the structure formation

We comment on a possibility for a chemical separation of charged and neutral species in a later epoch of structure formation. Depending on the virialization temperature of the collapsing structure, the ionization fraction after the virialization can be smaller than that during the gravitational collapse because of its high density. The baryon density in the late epoch is, on the other hand, much larger than that during the collapse. This requires much larger amplitude of magnetic field which causes the Lorentz force balanced by the friction force. For a fixed structure mass, the gravitation term [the first term in RHS of Eq. (19)] roughly scales as  $\propto \rho_b^{5/3} \propto (1 + \delta)^{5/3}$  [Eq. (22)]. On the other hand, when we roughly assume adiabatic contractions of charged species and magnetic domains during the collapse in the early epoch of structure formation, the Lorentz force term (the second term) scales as  $\propto B^2 / L_B \propto (1 + \delta)^{5/3}$ . Therefore, it is expected that if an ambipolar diffusion does not occur in the early structure formation epoch, it does

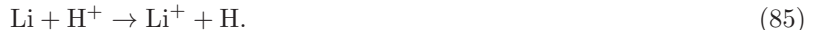
not also in later epochs as long as a magnetic field generation does not operate during the structure formation.

### B. Chemical reactions

Lithium atoms can be ionized through a reaction triggered by a ultraviolet (UV) photon:



They can be ionized also through a reaction triggered by an  $\text{H}^+$  ion which is generated by UV photons or cosmic rays:



The ionization potential of Li is  $I(\text{Li}) = 5.39$  eV which corresponds to the temperature  $T = 2I(\text{Li})/3 \sim 4 \times 10^4$  K. Some proportion of Li atoms can be also easily ionized by external UV sources or a gas heating at a virialization of structures. The  $\text{Li}^+$  ions produced secondarily in this way can then be trapped by magnetic field, and possibly remain behind forming structures. Such a contribution to a resulting lithium abundance in the collapsed structure, however, operates after the gravitational collapse of structure considered in this paper. They are then neglected here.

### C. Li abundance of MPS

Astronomical observations indicate primordial abundances of D [74],  $^3\text{He}$  [75],  $^4\text{He}$  [76, 77] consistent with those predicted in SBBN model. Primordial  $^7\text{Li}$  abundance is inferred from spectroscopic observations of metal-poor halo stars. We adopt  $\log(^7\text{Li}/\text{H}) = -12 + (2.199 \pm 0.086)$  determined with a 3D nonlocal thermal equilibrium model [12]. This estimation corresponds to the  $2\sigma$  range of

$$1.06 \times 10^{-10} < (^7\text{Li}/\text{H})^{\text{MPS}} < 2.35 \times 10^{-10}. \quad (86)$$

This Li abundance level is a factor of  $\sim 3$ – $4$  smaller than the SBBN prediction [2, 3], and the dispersion of observed Li abundance is small. Since the observed  $^7\text{Li}$  abundance is not so much different from the SBBN prediction, it is naturally expected that SBBN model successfully describes the outline of primordial light element synthesis. The Li abundances in MPSs can be affected by several physical processes operating after the BBN epoch. The abundance ratio of Li and H in MPSs is then expressed as

$$(\text{Li}/\text{H})^{\text{MPS}} = (\text{Li}/\text{H})^{\text{SBBN}} F^{\text{dep}}, \quad (87)$$

where  $(\text{Li}/\text{H})^{\text{SBBN}}$  is the abundance ratio in SBBN model, and  $F^{\text{dep}}$  is the depletion factor associated with 1) modified BBN models including exotic long-lived particles or changed expansion rate, 2) the structure formation as considered in this paper, 3) the virialization of the structure, 4) the formation of observed MPSs, and 5) the stellar processes in surfaces of MPSs occurring from the star formation until today.

Generally, cosmological processes change elemental abundances universally, while astrophysical processes change the abundances locally depending on physical environments of respective stars. It is, therefore, difficult to explain the discrepancy in  $^7\text{Li}$  abundance with astrophysical processes resulting in large dispersions.

The depletion factor from the chemical separation during the structure formation can be described by

$$\begin{aligned} F^{\text{dep}} &\equiv \frac{[(n_{^7\text{Li}} + n_{^7\text{Li}^+})/(n_{\text{H}} + n_{\text{H}^+})]_{\text{str}}}{[(n_{^7\text{Li}} + n_{^7\text{Li}^+})/(n_{\text{H}} + n_{\text{H}^+})]_{\text{uni}}} \\ &\approx \frac{\chi_{^7\text{Li},\text{uni}} + \chi_{\text{Li}^+,\text{str}}}{(\chi_{^7\text{Li}} + \chi_{^7\text{Li}^+})_{\text{uni}}}, \end{aligned} \quad (88)$$

where quantities with subscripts, "uni" and "str", are values of the homogeneous early universe after the cosmological recombination and those of the collapsed structure in the late universe, respectively. In the second line, it was assumed that the primordial ionization degree of hydrogen is negligibly small, i.e.,  $\chi_{\text{H}^+} \ll 1$ , and that values of the number ratio  $\chi_{^7\text{Li}}$  are equal in the homogeneous early universe and the structure. We suppose the initial abundance ratio of  $^7\text{Li}^+/^7\text{Li} \sim 1$  as suggested from a chemical history of homogeneous early universe [25]. The chemical separation via the ambipolar diffusion can only dilute the charged  $^7\text{Li}^+$ . A depletion factor is, therefore,  $1/2$  at minimum when the primordial  $^7\text{Li}^+$  is completely expelled from a structure. This factor would be smaller if the initial  $^7\text{Li}^+$  abundance for the gravitational structure formation is larger for some reason. For example, even a small intensity of ionizing photon

of  ${}^7\text{Li}$  would quickly transform  ${}^7\text{Li}$  to  ${}^7\text{Li}^+$  without absorption by neutral hydrogen (Sec. VIII B). The depletion factor would be larger, on the other hand, if the chemical separation is less efficient.

The Li abundance of MPSs may not be explained by the chemical separation only. In that case, we need another depletion mechanism. As an example, a rotationally induced mixing model [78, 79] for MPSs is chosen here since dispersions as well as depletion factors are predicted theoretically only in this model among stellar depletion models. Since the predicted depletion factor is proportional to the dispersion factor, the depletion factor is constrained with observed dispersions. Pinsonneault et al. estimated the depletion factor: “0.13 dex, with a 95 % range extending from 0.0 to 0.5 dex.” [79] This model then explains a part of the Li abundance discrepancy although the complete solution by this mechanism only seems almost impossible. The Li abundances in MPSs may, therefore, be explained by the combination of the ambipolar diffusion during the structure formation and the rotationally induced mixing in stars.

Stellar Li abundances in metal-poor globular clusters (GCs) have also been measured. For example, GC M4 was studied using high-resolution spectra with GIRAFFE at Very Large Telescope, and the Li abundance in turn-off stars is found to be  $\log({}^7\text{Li}/\text{H}) = -12 + (2.30 \pm 0.02 + 0.10)$  [80]. All Li abundances measured so far are summarized in Fig. 3 of Ref. [80], and they are consistent with abundances in metal-poor halo stars at present. If the ambipolar diffusion studied in this paper is the cause of the small Li abundances of MPSs, however, reduction factors of MPSs can reflect respective histories of parent structure for MPSs. In a modern model calculation for GC formation, the galaxy formation results from a continuous process of merging and accretion which is realized in a hierarchical structure formation scenario [81]. In the model, GCs form at densest regions of filaments in a large-scale structure.

#### D. Other constraint on PMF

Theoretical and observational constraints on the cosmic magnetic field have been summarized in Ref. [82]. The magnetic field strength in the interesting parameter region found in our study (Sec. VII) looks somewhat above the theoretical upper limit from the effect of dissipation of magnetic field through the processing by MHD turbulence. The propagation length of Alfvén wave is given by  $\lambda_B \sim v_A t$ , where  $v_A$  is the Alfvén speed. This length scale corresponds to “the size of largest processed eddies” [82] by MHD turbulence. The Alfvén speed during the matter dominated epoch of the homogeneous universe is given by  $v_A = B/\sqrt{\rho_b}$  with  $\rho_b \propto (1+z)^3$  the baryon density. The distance is then given by

$$\lambda_B \sim \left[ \frac{B_0}{\rho_{b0}^{1/2}} (1+z)^{1/2} \right] \left[ \frac{2}{3H_0\Omega_m^{1/2}(1+z)^{3/2}} \right] = \frac{2^{5/2}\pi^{1/2}}{3^{3/2}} \frac{B_0}{m_{\text{Pl}}H_0^2\Omega_b^{1/2}\Omega_m^{1/2}(1+z)}, \quad (89)$$

where  $m_{\text{Pl}}$  is the Planck mass. Consequently, the comoving propagation length  $\lambda_{B0} = \lambda_B(1+z)$  is constant.

Since the magnetic fields on scales less than  $\lambda_{B0}(B_0)$  decay, there is a maximum amplitude of magnetic field which escapes from this decay for a given  $\lambda_{B0}$ . From the above equation, an upper limit on the  $B_0$  value is derived as

$$B_0 \lesssim 4 \times 10^{-11} \text{ G} \left( \frac{h}{0.700} \right)^2 \left( \frac{\Omega_b}{0.0463} \right)^{1/2} \left( \frac{\Omega_m}{0.279} \right)^{1/2} \left( \frac{\lambda_{B0}}{10 \text{ kpc}} \right). \quad (90)$$

This upper limit is lower than the field value required for the chemical separation [Eqs. (81) and (83)] (by about one order of magnitude for  $\lambda_{B0} = 10 \text{ kpc}$ ). However, Eq (90) is just an order of estimate, and realistic limits should be derived in precise calculations in future. It is interesting that the upper limit caused by the MHD processing in the early universe is near to the interesting field strength. It indicates that relatively large magnetic field in the early universe may have been reduced by the MHD effect to the level which is most appropriate for the chemical separation causing the lithium problem.

During the gravitational collapse of structures, the Alfvén speed increases as  $\propto (1+\delta)^{1/6}$  if the dissipation of magnetic field is not operative. The dissipation scale in collapsed structures which are decoupled from the cosmic expansion is then given by

$$\lambda_B^{\text{str}}(z) \sim \frac{2^{5/2}\pi^2}{3^{3/2}} \frac{B_0(1+z)^{1/2}(1+\delta)^{1/6}}{m_{\text{Pl}}H_0^2\Omega_b^{1/2}\Omega_m^{1/2}(1+z)^{3/2}}. \quad (91)$$

The contraction increases the dissipation scale slightly. The MHD effect thus becomes effective in an environment of large density. Therefore, after the collapse, the magnetic field strength can be decreased further.



## IX. SUMMARY

We considered a possible effect of PMFs on motions of charged and neutral chemical species during the formation of first structures at redshift  $z = \mathcal{O}(10)$ . A gradient in the PMF in a direction perpendicular to the field direction is realized by an electric current of charged species in the direction perpendicular to both directions of the field lines and the gradient. The Lorentz force on the charged species then causes a velocity difference between charged and neutral species in the direction of the field gradient. Resultantly, a velocity of charged species can be different from that of neutral species which collapses gravitationally during the structure formation. Therefore,  ${}^7\text{Li}^+$  ions may have possibly escaped from gravitational collapse of early structures.

Calculations for fluid motions of charged and neutral species were performed through a simple estimation using fundamental fluid and electromagnetic equations. We assumed a gravitational contraction of neutral matter in a spherically symmetric structure. In addition, we utilized a cylindrical coordinate, and assumed a gradient of the altitudinal ( $z$ ) magnetic field component in the radial direction. Related physical quantities are listed, and their typical values are given in Sec. III. Some analytical equations are introduced in Appendix A.

When the amplitude of magnetic field is large enough, the charged fluid significantly decouples from the neutral fluid. Resultantly, it is possible that during the gravitational contraction of structure mainly composed of neutral hydrogen, contractions of proton, electron, and  ${}^7\text{Li}^+$  ion do not occur. Although fluid motions of charged chemical species are solved for only  $\text{H}^+$ ,  $e$ , and  ${}^7\text{Li}^+$  in this study, other charged species are expected to have similar motions. Because of large inductances of large astronomical structures, the generation of magnetic field is never efficient during the structure formation at  $z \sim 10$ . Therefore, only PMFs which existed from the start of the structure formation can trigger the chemical separation.

The chemical separation requires the gradient of magnetic field in a direction perpendicular to the field direction. Although such a gradient was assumed in the initial condition in this study, it may be produced associated with a density gradient during the gravitational contraction of structures without any initial gradient of the magnetic field.

Based on the calculated result of the chemical separation, we derived a parameter region for a successful chemical separation taking the structure mass, the turnaround redshift of the gravitational collapse, and the comoving Lorenz force, i.e.,  $B_{z0}^2/L_{B0}$ , as parameters. It was found that the parameter region can be constrained to be very narrow. If such a chemical separation has occurred during the structure formation, the primordial  ${}^7\text{Li}^+$  which was produced via the recombination of  ${}^7\text{Li}^{2+}$  but survived against its recombination during the cosmological recombination epoch possibly does not participate in the gravitational contraction. The abundance ratio of Li/H in early structures, which are progenitors of the Galaxy, can then be smaller than that inferred from SBBN model. The chemical separation may, therefore, be the cause of the Li problem of the MPSs.

Amplitudes of the PMFs needed for the chemical separation was estimated to be near to (somewhat smaller than) an upper limit determined from the effect of MHD turbulence on the decay of field amplitude. It may, therefore, be possible that the amplitude of PMFs generated through some mechanism operating in the extremely early universe was modulated to the value appropriate to the chemical separation.

### Appendix A: Solutions of variables from the force balance

#### 1. Drifts in the expanding universe

We consider two different cases of weak and strong Lorentz forces.

##### *a. Weak Lorentz force*

Firstly, we suppose that a magnetic field is so weak that momentum transfers from hydrogen to electron and proton through collisions result in very small velocity differences despite the existence of the weak Lorentz force. This case typically satisfies the condition  $B_z \ll (4\pi en_p \alpha_{pn} H L L_B)^{1/2}$  [cf. Eqs. (75) or (30)]. Because of effective scatterings between proton, electron, and neutral hydrogen, velocities of  $p$  and  $e$  are almost identical to that of neutral hydrogen, i.e.,  $\mathbf{v}_p = \mathbf{v}_e = \mathbf{v}_n$ . The force balances for  $p$  and  $e$  [Eqs. (4) and (5) with an assumption  $D/Dt = 0$  and a neglect of  $\nabla P_i$  terms] give the value of electric field:

$$\mathbf{E} \cong -\mathbf{v}_n \times \mathbf{B} = - \begin{pmatrix} 0 \\ v_{nz} B_r - v_{nr} B_z \\ 0 \end{pmatrix}, \quad (\text{A1})$$

where it was assumed that there is azimuthal components of neither magnetic field nor neutral hydrogen velocity.

### b. Strong Lorentz force

Secondly, we suppose that a magnetic field is strong, and the collisional momentum transfers between charged species and hydrogen with large radial relative velocities are counterbalanced by the Lorentz force, i.e.,  $B_z \sim (4\pi n_p \alpha_{pn} HLL_B)^{1/2}$ . The proton and electron then receive dynamical frictions of hydrogen with different amplitudes determined by momentum transfer cross sections. In such a case, proton and electron are promoted to start drifting in directions opposite to each other with velocities,  $\mathbf{v}_{Di} = \mathbf{F}_i \times \mathbf{B} / (Z_i e B^2)$ , where  $\mathbf{F}_i$  is the friction force [cf. Eqs. (4) and (5)]. The both drift directions are perpendicular to the direction of the friction force. Drift velocities of proton and electron are given by

$$\mathbf{v}_{Dp} = \frac{1}{B^2} \begin{pmatrix} [-\alpha_{pn} v_{p\phi} + \alpha_{pe} (v_{e\phi} - v_{p\phi})] B_z \\ [\alpha_{pn} (v_{nz} - v_{pz})] B_r - [\alpha_{pn} (v_{nr} - v_{pr})] B_z \\ [\alpha_{pn} v_{p\phi} - \alpha_{pe} (v_{e\phi} - v_{p\phi})] B_r \end{pmatrix}, \quad (\text{A2})$$

$$\mathbf{v}_{De} = -\frac{1}{B^2} \begin{pmatrix} -[\alpha_{en} v_{e\phi} + \alpha_{ep} (v_{e\phi} - v_{p\phi})] B_z \\ [\alpha_{en} (v_{nz} - v_{ez})] B_r - [\alpha_{en} (v_{nr} - v_{er})] B_z \\ [\alpha_{en} v_{e\phi} + \alpha_{ep} (v_{e\phi} - v_{p\phi})] B_r \end{pmatrix}. \quad (\text{A3})$$

However, these drifts never complete effectively because of large inductances of large astrophysical objects (Sec. V).

## 2. Equilibrium state

### a. Proton and electron

It is expected that equilibrium states had realized for bulk motions of chemical species and electromagnetic fields every time during the early epoch of structure formation. In the equilibrium state, force balance equations for proton ( $p$  or  $\text{H}^+$ : the dominant component of ion) and electron [Eqs. (6) and (7)] include nine unknown parameters: components of vectors  $\mathbf{E}$ ,  $\mathbf{v}_p$ , and  $\mathbf{v}_e$ . Because of nearly complete neutrality for local charge, fluid velocities of ion and electron should be approximately equal as for  $r$ - and  $z$ -components. The number of independent parameters is then reduced to be seven:  $E_r$ ,  $E_\phi$ ,  $E_z$ ,  $v_{pr} = v_{er}$ ,  $v_{pz} = v_{ez}$ ,  $v_{p\phi}$ , and  $v_{e\phi}$ .

The conditions have been imposed additionally:  $v_{n\phi} = 0$  and  $B_\phi = 0$ . Three equations for  $E_r$ ,  $E_\phi$ , and  $E_z$  are then obtained:

$$E_r = -v_{p\phi} B_z - \alpha_{pn} (v_{nr} - v_{pr}) = -v_{e\phi} B_z + \alpha_{en} (v_{nr} - v_{pr}), \quad (\text{A4})$$

$$E_\phi = -(v_{pz} B_r - v_{pr} B_z) + \alpha_{pn} v_{p\phi} - \alpha_{pe} (v_{e\phi} - v_{p\phi}) = -(v_{pz} B_r - v_{pr} B_z) - \alpha_{en} v_{e\phi} - \alpha_{pe} (v_{e\phi} - v_{p\phi}), \quad (\text{A5})$$

$$E_z = v_{p\phi} B_r - \alpha_{pn} (v_{nz} - v_{pz}) = v_{e\phi} B_r + \alpha_{en} (v_{nz} - v_{pz}). \quad (\text{A6})$$

From the second equality of Eq. (A5), we instantaneously find

$$v_{e\phi} = -\frac{\alpha_{pn}}{\alpha_{en}} v_{p\phi}. \quad (\text{A7})$$

From the second equalities of Eqs. (A4) and (A6),  $v_{pr}$  and  $v_{pz}$  values are given, respectively:

$$v_{pr} = v_{nr} + \frac{B_z}{\alpha_{en}} v_{p\phi}, \quad (\text{A8})$$

$$v_{pz} = v_{nz} - \frac{B_r}{\alpha_{en}} v_{p\phi}. \quad (\text{A9})$$

Insertion of Eqs. (A8) and (A9) in the first equality of Eq. (A5) leads to an expression for the parameter  $v_{p\phi}$ :

$$v_{p\phi} = \frac{\alpha_{en} (E_\phi + B_r v_{nz} - B_z v_{nr})}{B^2 + \alpha_{en} \alpha_{pn} + \alpha_{pe} (\alpha_{en} + \alpha_{pn})}. \quad (\text{A10})$$

The  $v_{p\phi}$  value is given by the rotation of  $B$  field [Eq. (32)]. We thus have seven equations for seven variables. The solutions can, therefore, be obtained.

b. General singly-ionized ions

From the force equation for singly-ionized ion ( $i = \text{H}^+, \text{Li}^+, \dots$ ), the electric field is given by

$$\mathbf{E} = -\mathbf{v}_i \times \mathbf{B} - \frac{\rho_i (\mathbf{v}_n - \mathbf{v}_i)}{\tau_{in} \epsilon n_i} - \frac{\rho_i (\mathbf{v}_e - \mathbf{v}_i)}{\tau_{ie} \epsilon n_i}. \quad (\text{A11})$$

The left-hand side corresponds to the term of electric field, and the first, second and third terms in the RHS correspond to the Lorentz force, the frictions of H and electron, respectively. The friction of proton is neglected in the force equation for  $i \neq p$  since the friction parameter  $\alpha_{ip}$  is smaller than  $\alpha_{ie}$  by a factor of  $\sim m_e/m_p$  [cf. Eq. (62)]. For the case of  ${}^7\text{Li}^+$ , the force balance equation is somewhat different from that of proton because of differences in the ion masses and the momentum transfer cross sections.

We do not assume the condition of charge neutrality since abundance of  $i$  can be negligibly small (for example, the primordial number ratio of  ${}^7\text{Li}^+/\text{H}$  is about  $2.6 \times 10^{-10}$  [25]). We have assumed that  $v_{n\phi} = 0$  and  $B_\phi = 0$ . Three equations for  $E_r$ ,  $E_\phi$ , and  $E_z$  are then obtained:

$$E_r = -v_{i\phi} B_z - \alpha_{in} (v_{nr} - v_{ir}) - \alpha_{ie} (v_{er} - v_{ir}), \quad (\text{A12})$$

$$E_\phi = -(v_{iz} B_r - v_{ir} B_z) + \alpha_{in} v_{i\phi} - \alpha_{ie} (v_{e\phi} - v_{i\phi}), \quad (\text{A13})$$

$$E_z = v_{i\phi} B_r - \alpha_{in} (v_{nz} - v_{iz}) - \alpha_{ie} (v_{ez} - v_{iz}). \quad (\text{A14})$$

Using these three equations with values of  $\mathbf{E}$  and  $\mathbf{v}_e$  derived in Appendix A 2 a, the velocity of  $i$  is solved:

$$\begin{pmatrix} v_{ir} \\ v_{i\phi} \\ v_{iz} \end{pmatrix} = \frac{1}{\alpha_i (\alpha_i^2 + B_r^2 + B_z^2)} \begin{pmatrix} \alpha_i^2 + B_r^2 & \alpha_i B_z & B_r B_z \\ -\alpha_i B_z & \alpha_i^2 & \alpha_i B_r \\ B_r B_z & -\alpha_i B_r & \alpha_i^2 + B_z^2 \end{pmatrix} \left[ \begin{pmatrix} E_r \\ E_\phi \\ E_z \end{pmatrix} + \begin{pmatrix} \alpha_{in} v_{nr} + \alpha_{ie} v_{er} \\ \alpha_{ie} v_{e\phi} \\ \alpha_{in} v_{nz} + \alpha_{ie} v_{ez} \end{pmatrix} \right], \quad (\text{A15})$$

where  $\alpha_i \equiv \alpha_{in} + \alpha_{ie}$  was defined.

### 3. Typical case for an effective chemical separation at the turnaround

As a guide, we define a typical case of effective chemical separation in which the radial velocity difference between charged and neutral species is exactly equal to the recession velocity at the turnaround. The velocity difference is determined from the balance between the Lorentz force and the friction by neutral hydrogen in the  $r$ -direction. We assume a strong magnetic field in  $z$ -direction, i.e.,  $B_z \gg \alpha_{ij}, B_r$ . In this case, ions and electron possibly do not move to the structure center, and their radial velocities can be as large as the cosmic recession velocity. Velocities of charged species at the radius  $r_p$  are then matched to the cosmic recession velocity, i.e.,

$$v_{pr} = H r_p. \quad (\text{A16})$$

The electric field and velocities of proton are determined accordingly:

Eqs. (A10) and (A9), respectively, give relations of

$$v_{p\phi} = \frac{\alpha_{en}}{B_z} (H r_p - v_{nr}), \quad (\text{A17})$$

$$v_{pz} = v_{nz} - \frac{B_r}{B_z} (H r_p - v_{nr}) \sim v_{nz}. \quad (\text{A18})$$

The equilibrium electric field is then derived:

$$E_r = (\alpha_{pn} - \alpha_{en}) (H r_p - v_{nr}), \quad (\text{A19})$$

$$E_\phi = \left[ \frac{\alpha_{en} \alpha_{pn} + \alpha_{pe} (\alpha_{en} + \alpha_{pn}) + B_r^2}{B_z} \right] (H r_p - v_{nr}) - B_r v_{nz} + B_z H r_p, \quad (\text{A20})$$

$$E_z = -(\alpha_{pn} - \alpha_{en}) \frac{B_r}{B_z} (H r_p - v_{nr}). \quad (\text{A21})$$

Under the assumption of Eq. (A16), the velocity of the singly charged ion  $i$  [Eq. (A15)] has an approximate form of

$$v_{ir} \approx H r_p, \quad (\text{A22})$$

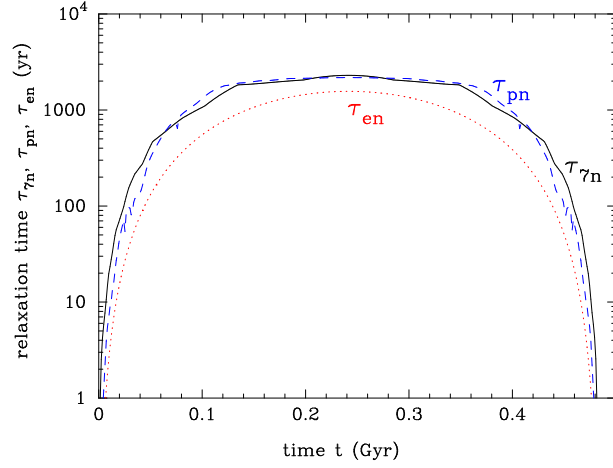


FIG. 8: Relaxation times  $\tau_{7n}$  (solid line) for  ${}^7\text{Li}^+$ ,  $\tau_{pn}$  (dashed line) for  $\text{H}^+$ , and  $\tau_{en}$  (dotted line) for  $e^-$  through collisions with hydrogen as a function of cosmic time  $t$  for both Cases 1 and 2.

$$v_{i\phi} \approx \frac{\alpha_{in} - \alpha_{pn} + \alpha_{en}}{B_z} (Hr_p - v_{nr}), \quad (\text{A23})$$

$$v_{iz} \approx v_{nz} - \frac{B_r}{B_z} (Hr_p - v_{nr}). \quad (\text{A24})$$

## Appendix B: Detailed results of physical variables

In this section, we show supplemental results of calculations performed in Sec. IV.

### 1. Relaxation time scales

Figure 8 shows relaxation times  $\tau_{7n}$  (solid line) for  ${}^7\text{Li}^+$ ,  $\tau_{pn}$  (dashed line) for  $\text{H}^+$ , and  $\tau_{en}$  (dotted line) for  $e^-$  through collisions with hydrogen as a function of cosmic time  $t$ . In this calculation, it is assumed that a relaxation time  $\tau_{ij}$  is the time it takes a species  $i$  to change its velocity toward that of  $j$  until a difference in velocities of  $i$  and  $j$  becomes the range within the thermal CM velocity of the  $i+j$  system. When the velocity difference,  $|\mathbf{v}_i - \mathbf{v}_j|$ , is smaller than the thermal velocity, the  $\tau_{ij}$  value is approximated by that evaluated at the thermal velocity. In the present calculations for Case 1 and 2, any velocity differences were found to be smaller than thermal velocities at almost all position and time. The relaxation time scales are then determined only from the thermal velocity in the structure, and do not depend on radius.

Since the relaxation time is inversely proportional to the target number density [Eq. (51)], the  $\tau_{ij}$  values increases during the expanding phase ( $t \leq 0.242$  Gyr), while it progressively becomes smaller during the contracting phase ( $t \geq 0.242$  Gyr). Cross sections are taken using linear interpolations of adopted data. This approximation causes a non-smooth behavior in the  $\tau_{7n}$  curve. In addition to a similar non-smoothness, zigzags are seen in the  $\tau_{pn}$  curve, which result from fluctuations in the cross section. The smooth shape of the  $\tau_{en}$  curve reflects the constant cross section assumed for CM energy smaller than the lowest energy data point  $\sim 15$  meV.

Figure 9 shows the relaxation time  $\tau_{pe}$  of  $\text{H}^+$  as a function of radius for Case 1 (left panel) and Case 2 (right panel). Solid and dashed lines correspond to values inside and outside the structure, respectively. In whole the calculation time, the relative velocity of proton and electron is given by the thermal velocity since the relative fluid velocity is smaller than the thermal velocity. The  $\tau_{pe}$  values at large radii are almost constant with the increasing time, which originate from a constant reaction rate for a given thermal velocity and a constant density of electron. The thermal velocity is assumed to be proportional to the square root of gas temperature  $T \propto \rho_n^{2/3}$ , while the proton and electron number densities scale as  $n_i \propto \rho_i$ . The relaxation time is then given by  $\tau_{pe} = (m_p/m_e)\tau_{ep} \propto T^{3/2}/n_p \propto \rho_n/\rho_p$  [cf. Eqs. (56) and (59)]. Inside the structure, this quantity increases with time since the number abundances of proton and other charged species decrease (Fig. 3).

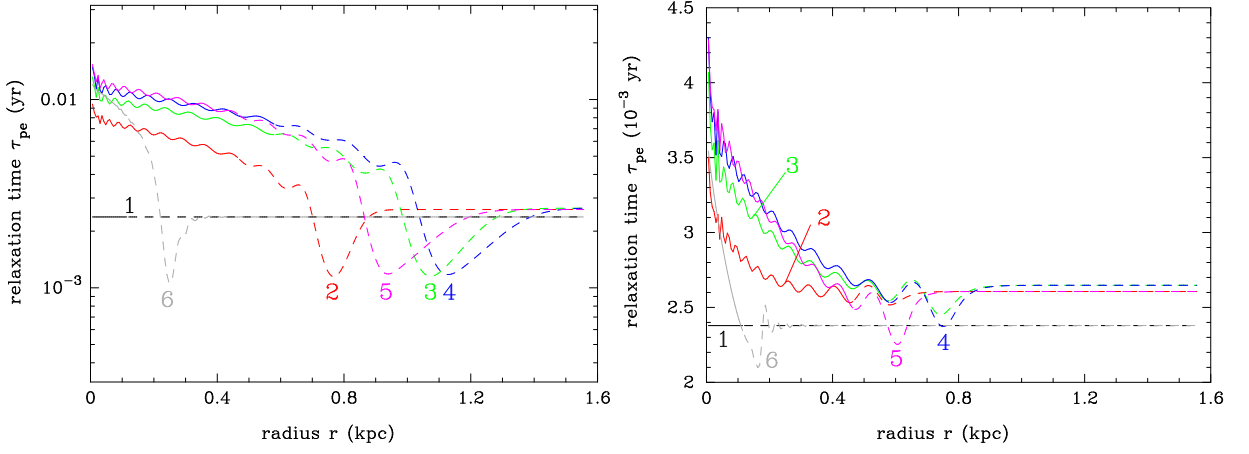


FIG. 9: Relaxation time  $\tau_{pe}$  of  $H^+$  through collisions with electron as a function of radius for Case 1 (left panel) and Case 2 (right panel) at  $t=9.29$  Myr (1), 102 Myr (2), 195 Myr (3), 288 Myr (4), 381 Myr (5), and 474 Myr (6). Solid and dashed lines correspond to values inside and outside the structure, respectively.

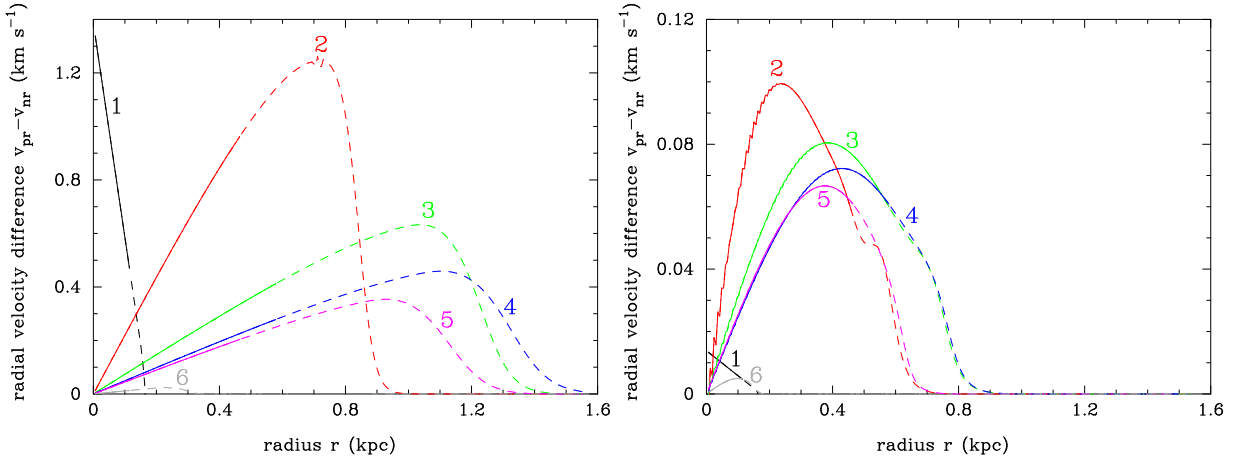


FIG. 10: Radial velocity difference between  $H^+$  and  $H$ ,  $v_{pr} - v_{nr}$ , as a function of radius for Case 1 (left panel) and Case 2 (right panel) at  $t=9.29$  Myr (1), 102 Myr (2), 195 Myr (3), 288 Myr (4), 381 Myr (5), and 474 Myr (6). Solid and dashed lines correspond to values inside and outside the structure, respectively.

## 2. Relative velocities

Figure 10 shows the difference in radial velocities of  $H^+$  and  $H$ , i.e.,  $v_{pr} - v_{nr}$ , as a function of radius for Case 1 (left panel) and Case 2 (right panel). Solid and dashed lines correspond to values inside and outside the structure, respectively. The difference in radial velocities of  ${}^7\text{Li}^+$  and  $H$ , i.e.,  $v_{7r} - v_{nr}$  is the same as that of  $H^+$  and  $H$ . The conditions,  $B_z \gg \alpha_{ie} \gg \alpha_{in}, B_r$  (for  $i = p$  and  ${}^7\text{Li}^+$ ) and  $v_{jr}, v_{jz} \gg v_{j\phi}$  (for any species  $j$ ), are satisfied in the present case. Under these conditions, the situation of  $v_{7r} \sim v_{pr}$  results [see Eq. (A22)]. Strictly ions such as the  ${}^7\text{Li}^+$  ion have radial velocities very slightly different from that of proton under an electric field in which radial motions of proton and electron are balanced. [84] The velocity difference is larger in Case 1 than in Case 2. The time evolution is also different since the movement of charged species is larger and the evolution of  $B_z$  value in small radii is more significant for the larger magnetic field in Case 1.

Figure 11 shows the azimuthal velocity of proton  $v_{p\phi}$  as a function of radius for Case 1 (left panel) and Case 2 (right panel). Solid and dashed lines correspond to values inside and outside the structure, respectively. This quantity scales as  $(\nabla \times \mathbf{B})_\phi$  [Eq. (32)]. Velocities at small radii are then larger since a gradient of  $B_z$  is assumed at small radii in the initial condition. The velocity is roughly independent of the time or the hydrogen density if there is no weakening of magnetic field (cf. Fig. 4). This is because  $v_{p\phi} \propto (B_z/L_B)/n_p \propto 1/(L_B^3 n_p)$  is nearly constant. The movement of charge species relative to neutral hydrogen, however, gradually reduces the gradient of the magnetic field,  $\partial_r B_z$ . This

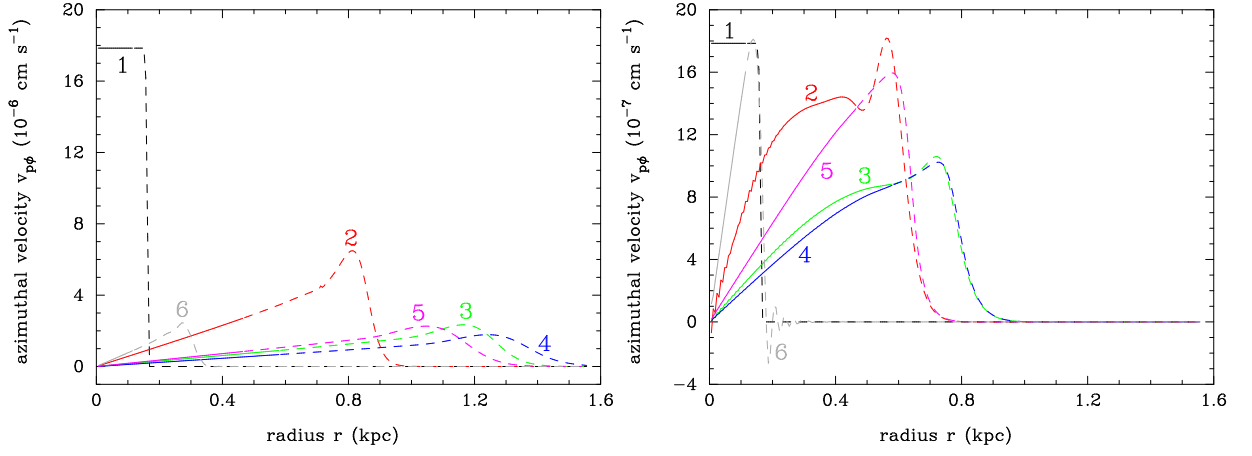


FIG. 11: Azimuthal velocity of proton  $v_{p\phi}$  as a function of radius for Case 1 (left panel) and Case 2 (right panel) at  $t=9.29$  Myr (1), 102 Myr (2), 195 Myr (3), 288 Myr (4), 381 Myr (5), and 474 Myr (6). Solid and dashed lines correspond to values inside and outside the structure, respectively.

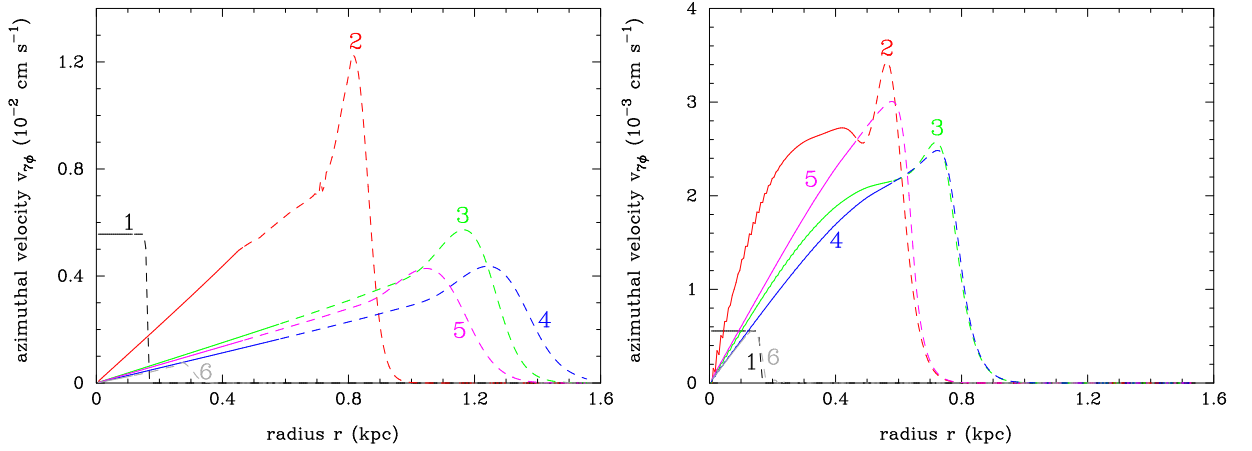


FIG. 12: Azimuthal velocity of  ${}^7\text{Li}^+$   $v_{7\phi}$  as a function of radius for Case 1 (left panel) and Case 2 (right panel) at  $t=9.29$  Myr (1), 102 Myr (2), 195 Myr (3), 288 Myr (4), 381 Myr (5), and 474 Myr (6). Solid and dashed lines correspond to values inside and outside the structure, respectively.

effect reduces the velocity as a function of time. Shapes of the curves are similar between Cases 1 and 2. Amplitudes and the time evolutions of the velocities are, however, different for the same reason described for Fig. 10.

Figure 12 shows the azimuthal velocity of  ${}^7\text{Li}^+$   $v_{7\phi}$  as a function of radius for Case 1 (left panel) and Case 2 (right panel). Solid and dashed lines correspond to values inside and outside the structure, respectively. This quantity reflects the force balance as described in Eq. (A15). Because of the conditions,  $B_z \gg \alpha_{ie} \gg \alpha_{in}, B_r$  (for  $i = p$  and  ${}^7\text{Li}^+$ ) and  $v_{jr}, v_{jz} \gg v_{j\phi}$  (for any species  $j$ ), the azimuthal velocity has a limit value of  $v_{7\phi} = [(\alpha_{pn} + \alpha_{in})/B_z](v_{pr} - v_{nr})$ , which is different from both of  $v_{p\phi}$  and  $v_{e\phi}$ .

### 3. Electric field

Figure 13 shows the radial component of electric field  $E_r$  as a function of radius for Case 1 (left panel) and Case 2 (right panel). Solid and dashed lines correspond to values inside and outside the structure, respectively. The  $E_r$  value is given by

$$E_r = (\alpha_{pn} - \alpha_{en})(v_{pr} - v_{nr})$$

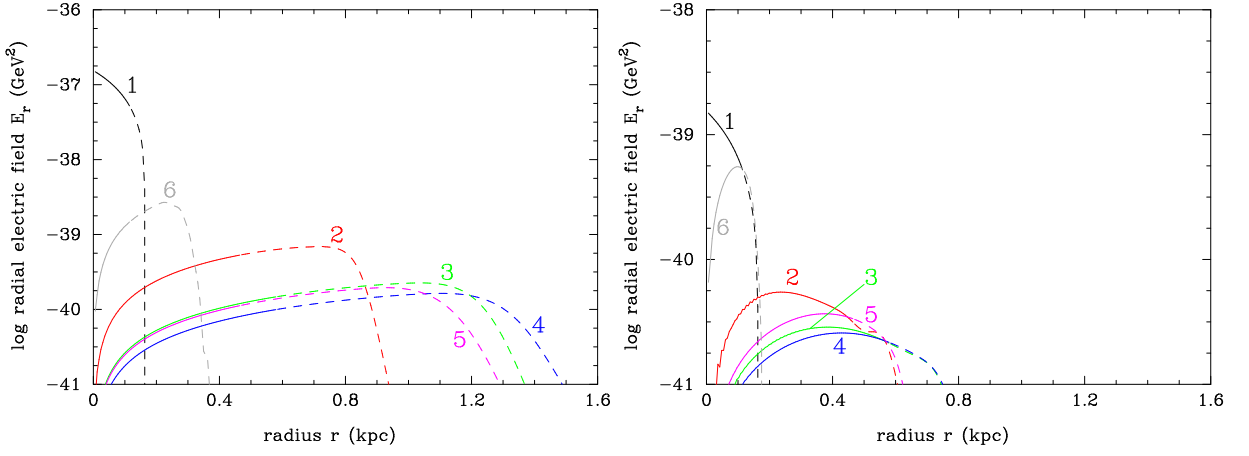


FIG. 13: Radial electric field as a function of radius for Case 1 (left panel) and Case 2 (right panel) at  $t=9.29$  Myr (1), 102 Myr (2), 195 Myr (3), 288 Myr (4), 381 Myr (5), and 474 Myr (6). Solid and dashed lines correspond to values inside and outside the structure, respectively.

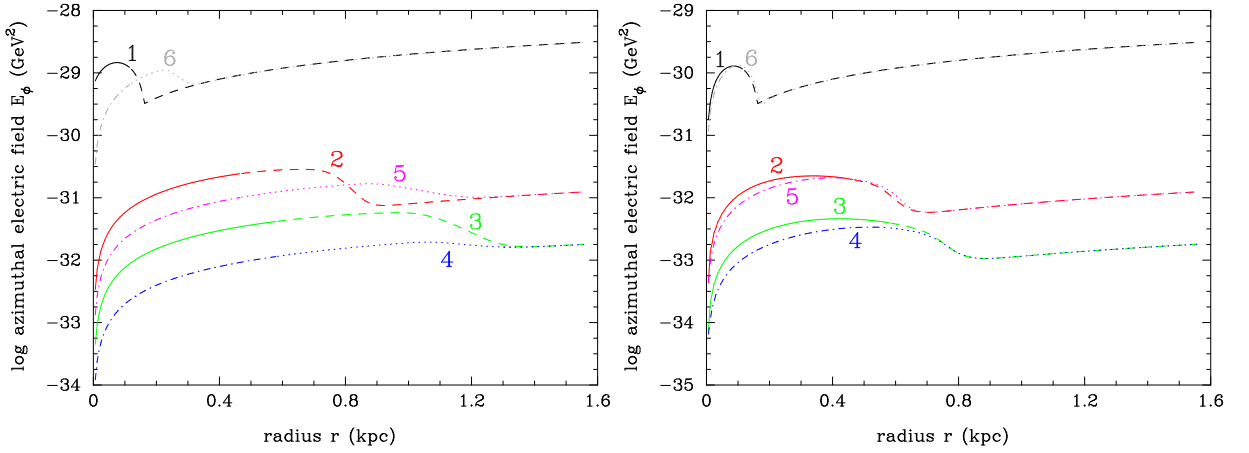


FIG. 14: Azimuthal electric field as a function of radius for Case 1 (left panel) and Case 2 (right panel) at  $t=9.29$  Myr (1), 102 Myr (2), 195 Myr (3), 288 Myr (4), 381 Myr (5), and 474 Myr (6). Solid and dashed lines correspond to positive values inside and outside the structure, respectively. Dot-dashed and dotted lines correspond to negative values inside and outside the structure, respectively.

$$\begin{aligned}
 &= \frac{1}{e} \left( \frac{m_p}{\tau_{pn}} - \frac{m_e}{\tau_{en}} \right) \frac{\tau_{np}}{\rho_n} \frac{\partial_z B_r - \partial_r B_z}{4\pi} B_z \\
 &\propto \frac{-(\partial_r B_z) B_z}{\rho_n}, \tag{B1}
 \end{aligned}$$

where Eqs. (A4) and (A8) were used in the first equality, and Eqs. (20) and (30) were used in the second equality. It thus scales as  $\propto (\partial_r B_z) B_z / \rho_n$ , and decreases during the expanding phase (curves 1–3), while it increases during the contracting phase (curves 4–6).

Figure 14 shows the azimuthal component of electric field  $E_\phi$  as a function of radius for Case 1 (left panel) and Case 2 (right panel). Solid and dashed lines correspond to positive values inside and outside the structure, respectively. Dot-dashed and dotted lines correspond to negative values inside and outside the structure, respectively. In the case of strong magnetic field of  $B_z \gg \alpha_{ij}, B_r$ , the relation  $E_\phi \propto v_{pr} B_z$  holds in this calculation [Eq. (A5)]. According to the relation, the  $E_\phi$  value decreases with time. The radial velocity is large in the early epoch (curve 1), which is approximately equal to the cosmic expansion velocity. The velocity is negative and its amplitude is large in the late epoch (curve 6), which is given by free fall velocity in the structure.



### Acknowledgments

We are grateful to Tomoaki Ishiyama for instructive information on structure formation. This work has been supported by Grant-in-Aid for Scientific Research from the Ministry of Education, Science, Sports, and Culture (MEXT), Japan, No.22540267 and No.21111006, and by World Premier International Research Center Initiative (WPI Initiative), MEXT, Japan.

- 
- [1] B. D. Fields, *Ann. Rev. Nucl. Part. Sci.* **61**, 47 (2011).
  - [2] A. Coc, S. Goriely, Y. Xu, M. Saimpert and E. Vangioni, *Astrophys. J.* **744**, 158 (2012).
  - [3] A. Coc, J. -P. Uzan and E. Vangioni, arXiv:1307.6955 [astro-ph.CO].
  - [4] J. Melendez and I. Ramirez, *Astrophys. J.* **615**, L33 (2004).
  - [5] M. Asplund, D. L. Lambert, P. E. Nissen, F. Primas and V. V. Smith, *Astrophys. J.* **644**, 229 (2006).
  - [6] F. Spite and M. Spite, *Astron. Astrophys.* **115**, 357 (1982).
  - [7] S. G. Ryan, T. C. Beers, K. A. Olive, B. D. Fields and J. E. Norris, *Astrophys. J.* **530**, L57 (2000).
  - [8] P. Bonifacio, P. Molaro and T. Sivarani *et al.*, *Astron. Astrophys.* **462**, 851 (2007).
  - [9] J. R. Shi, T. Gehren, H. W. Zhang, J. L. Zeng and G. Zhao, *Astron. Astrophys.* **465**, 587 (2007).
  - [10] W. Aoki, P. S. Barklem, T. C. Beers, N. Christlieb, S. Inoue, A. E. G. Perez, J. E. Norris and D. Carollo, *Astrophys. J.* **698**, 1803 (2009).
  - [11] J. I. G. Hernandez, P. Bonifacio, E. Caffau, M. Steffen, H. -G. Ludwig, N. T. Behara, L. Sbordone and R. Cayrel *et al.*, arXiv:0909.0983 [astro-ph.GA].
  - [12] L. Sbordone, P. Bonifacio, E. Caffau, H. -G. Ludwig, N. T. Behara, J. I. G. Hernandez, M. Steffen and R. Cayrel *et al.*, *Astron. Astrophys.* **522**, A26 (2010).
  - [13] L. Monaco, P. Bonifacio, L. Sbordone, S. Villanova and E. Pancino, *Astron. Astrophys.* **519**, L3 (2010).
  - [14] L. Monaco, S. Villanova, P. Bonifacio, E. Caffau, D. Geisler, G. Marconi, Y. Momany and H. -G. Ludwig, *Astron. Astrophys.* **539**, A157 (2012).
  - [15] A. Mucciarelli, M. Salaris and P. Bonifacio, *Mon. Not. R. Astron. Soc.* **419**, 2195 (2012).
  - [16] D. N. Spergel *et al.* [WMAP Collaboration], *Astrophys. J. Suppl.* **148**, 175 (2003).
  - [17] D. N. Spergel *et al.* [WMAP Collaboration], *Astrophys. J. Suppl.* **170**, 377 (2007).
  - [18] D. Larson, J. Dunkley, G. Hinshaw, E. Komatsu, M. R. Nolte, C. L. Bennett, B. Gold and M. Halpern *et al.*, *Astrophys. J. Suppl.* **192**, 16 (2011).
  - [19] G. Hinshaw *et al.* [WMAP Collaboration], *Astrophys. J. Suppl.* **208**, 19 (2013).
  - [20] A. Dalgarno and S. Lepp, *Astrochemistry* **120**, 109 (1987).
  - [21] S. Lepp and J. M. Shull, *Astrophys. J.* **280**, 465 (1984).
  - [22] P. J. E. Peebles and R. H. Dicke, *Astrophys. J.* **154**, 891 (1968).
  - [23] D. Galli and F. Palla, *Astron. Astrophys.* **335**, 403 (1998).
  - [24] W. C. Saslaw and D. Zipoy, *Nature* **216**, 976 (1967).
  - [25] P. Vonlanthen, T. Rauscher, C. Winteler, D. Puy, M. Signore and V. Dubrovich, *Astron. Astrophys.* **503**, 47 (2009).
  - [26] D. Grasso and H. R. Rubinstein, *Phys. Rept.* **348**, 163 (2001).
  - [27] L. Biermann, *Zeitschrift Naturforschung Teil A* **5**, 65 (1950).
  - [28] P. F. Browne, *Astrophys. Lett.* **2**, 217 (1968).
  - [29] P. F. Browne, *Astrophys. Space Sci* **87**, 407 (1982).
  - [30] P. F. Browne, *Astron. Astrophys.* **144**, 298 (1985).
  - [31] E. R. Harrison, *Astrophys. Lett.* **3**, 133 (1969).
  - [32] F. Hoyle and J. G. Ireland, *Mon. Not. R. Astron. Soc.* **120**, 173 (1960).
  - [33] L. Jr. Spitzer, *Astron. J.* **53**, 117 (1948).
  - [34] L. M. Widrow, *Rev. Mod. Phys.* **74**, 775 (2002).
  - [35] L. M. Widrow, D. Ryu, D. R. G. Schleicher, K. Subramanian, C. G. Tsagas and R. A. Treumann, *Space Sci. Rev.* **166**, 37 (2012).
  - [36] K. Ichiki, K. Takahashi, N. Sugiyama, H. Hanayama and H. Ohno, astro-ph/0701329.
  - [37] E. Fenu, C. Pitrou and R. Maartens, *Mon. Not. R. Astron. Soc.* **414**, 2354 (2011).
  - [38] K. Ichiki, K. Takahashi, H. Ohno, H. Hanayama and N. Sugiyama, *Science*, **311**, 827 (2006).
  - [39] K. Takahashi, K. Ichiki and N. Sugiyama, *Phys. Rev. D* **77**, 124028 (2008).
  - [40] K. Takahashi, K. Ichiki, H. Ohno and H. Hanayama, *Phys. Rev. Lett.* **95**, 121301 (2005).
  - [41] S. Maeda, K. Takahashi and K. Ichiki, *JCAP* **1111**, 045 (2011).
  - [42] S. Matarrese, S. Mollerach, A. Notari and A. Riotto, *Phys. Rev. D* **71**, 043502 (2005).
  - [43] E. R. Harrison, *Mon. Not. R. Astron. Soc.* **147**, 279 (1970).
  - [44] M. J. Rees and M. Reinhardt, *Astron. Astrophys.* **19**, 189 (1972).
  - [45] I. Wasserman, *Astrophys. J.* **224**, 337 (1978).
  - [46] P. Coles, *Comments Astrophys.* **16**, 45 (1992).
  - [47] H. Alfven, *Cosmic plasma, Astrophysics and Space Science Library*, 82 (D. Reidel, Dordrecht, Netherlands, 1981), Chaps.

III and V.

- [48] G. E. Ciolek and T. C. Mouschovias, *Astrophys. J.* **418**, 774 (1993).
- [49] G. E. Ciolek and T. C. Mouschovias, *Astrophys. J.* **425**, 142 (1994).
- [50] T. C. Mouschovias, G. E. Ciolek, and S. A. Morton, *Mon. Not. R. Astron. Soc.* **415**, 1751 (2011).
- [51] S. Basu and T. C. Mouschovias, *Astrophys. J.* **432**, 720 (1994).
- [52] P. J. E. Peebles, *Principles of Physical Cosmology* (Princeton University Press, Princeton, NJ, 1993), p176–178.
- [53] A. Loeb and M. Zaldarriaga, *Phys. Rev. Lett.* **92**, 211301 (2004).
- [54] J. A. Peacock, *Cosmological Physics* (Cambridge University Press, Cambridge, UK, 1999), p488.
- [55] G. Audi, A. H. Wapstra, and C. Thibault, *Nucl. Phys. A* **729**, 337 (2003).
- [56] A. H. Wapstra, G. Audi, and C. Thibault, *Nucl. Phys. A* **729**, 129 (2003).
- [57] W.C. Martin, A. Musgrove, S. Kotochigova, and J.E. Sansonetti (2011), Ground Levels and Ionization Energies for the Neutral Atoms (version 1.3). [Online] Available: <http://physics.nist.gov/IonEnergy> [Tuesday, 16-Oct-2012 08:25:15 EDT]. National Institute of Standards and Technology, Gaithersburg, MD.
- [58] W. R. Johnson and G. Soff, *At. Data Nucl. Data Tables* **33**, 405 (1985).
- [59] C.-J. Lorenzen and K. Niemax, *J. Phys. B* **15**, L139 (1982).
- [60] A. E. Glassgold, P. S. Krstić, and D. R. Schultz, *Astrophys. J.* **621**, 808 (2005).
- [61] D. R. Schultz, P. S. Krstic, T. G. Lee, and J. C. Raymond, *Astrophys. J.* **678**, 950 (2008).
- [62] P. S. Krstić and D. R. Schultz, *Phys. Plasmas* **16**, 053503 (2009).
- [63] D. J. Fixsen, *Astrophys. J.* **707**, 916 (2009).
- [64] M. Kawasaki and M. Kusakabe, *Phys. Rev. D* **86**, 063003 (2012).
- [65] A. P. Serebrov and A. K. Fomin, *Phys. Rev. C* **82**, 035501 (2010).
- [66] B. L. Moiseiwitsch, in *Atomic and Molecular Processes* edited by D. R. Bates (Academic, New York, 1962), p280.
- [67] L. Spitzer, *Physics of Fully Ionized Gases* (Dover, New York, 2006), Chap. 5.
- [68] M. Tegmark, J. Silk, M. J. Rees, A. Blanchard, T. Abel and F. Palla, *Astrophys. J.* **474**, 1 (1997).
- [69] T. Ishiyama (2013; private communications).
- [70] H. Alfvén, *Cosmic plasma, Astrophysics and Space Science Library*, 82 (D. Reidel, Dordrecht, Netherlands, 1981), p82–84.
- [71] H. Alfvén, *Cosmic plasma, Astrophysics and Space Science Library*, 82 (D. Reidel, Dordrecht, Netherlands, 1981), p86–88.
- [72] H. Alfvén, *Cosmic plasma, Astrophysics and Space Science Library*, 82 (D. Reidel, Dordrecht, Netherlands, 1981), p114–115.
- [73] L. C. Woods, *Physics of Plasmas* (Wiley-VCH, Weinheim, Germany, 2004), Chap. IV.
- [74] M. Pettini and R. Cooke, *Mon. Not. Roy. Astron. Soc.* **425**, 2477 (2012).
- [75] T. M. Bania, R. T. Rood and D. S. Balser, *Nature* **415**, 54 (2002).
- [76] Y. I. Izotov and T. X. Thuan, *Astrophys. J.* **710**, L67 (2010).
- [77] E. Aver, K. A. Olive and E. D. Skillman, *JCAP* **1005**, 003 (2010).
- [78] M. H. Pinsonneault, T. P. Walker, G. Steigman and V. K. Narayanan, *Astrophys. J.* **527**, 180 (2002).
- [79] M. H. Pinsonneault, G. Steigman, T. P. Walker and V. K. Narayanans, *Astrophys. J.* **574**, 398 (2002).
- [80] A. Mucciarelli, M. Salaris, L. Lovisi, F. R. Ferraro, S. Lucatello and R. G. Gratton, *Mon. Not. R. Astron. Soc.* **412**, 81 (2011).
- [81] A. V. Kravtsov and O. Y. Gnedin, *Astrophys. J.* **623**, 650 (2005).
- [82] R. Durrer and A. Neronov, *Astron. Astrophys. Rev.* **21**, 62 (2013).
- [83] WWW: <http://lambda.gsfc.nasa.gov>.
- [84] Inhomogeneous chemical abundances in cosmic plasma including solar flares have been considered [70]. One of their mechanisms is the mass dependent gravitational drift resulting in isotope separation of single element. In this study, we treat species-dependent dynamical frictions operating in low density plasma with a very small fraction of ionized hydrogen as realized in the early universe. Although the frictions induce a chemical separation as one kind of separations, its effect is negligible because of a strong electric coupling of positively charged ions and negatively charged electron.